International Journal of Heat and Fluid Flow 54 (2015) 220–235

Contents lists available at ScienceDirect

International Journal of Heat and Fluid Flow

journal homepage: www.elsevier.com/locate/ijhff

A Reynolds stress model for turbulent flow of homogeneous polymer solutions

M. Masoudian [a,*], K. Kim [b], F.T. Pinho [a], R. Sureshkumar [c]

[a] Transport Phenomena Research Center, Faculty of Engineering, University of Porto, Rua Dr. Roberto Frias s/n, 4200-465 Porto, Portugal
[b] Department of Mechanical Engineering, Hanbat National University, 125 Dongseo-daero, Yuseong-gu, Daejeon 305-701, South Korea
[c] Department of Biomedical and Chemical Engineering, Department of Physics, Syracuse University, NY 13244, USA

ARTICLE INFO

Article history:
Received 24 October 2014
Received in revised form 10 April 2015
Accepted 27 May 2015

Keywords:
Drag reduction
FENE-P fluid
Viscoelastic DNS
Viscoelastic RANS model

ABSTRACT

Using *a priori* analyses of direct numerical simulation (DNS) data, a Reynolds stress model (RSM) is developed to account for the influence of polymer additives on turbulent flow over a wide range of flow conditions. The Finitely Extensible Nonlinear Elastic-Peterlin (FENE-P) rheological constitutive model is utilized to evaluate the polymer contribution to the stress tensor. Thirteen DNS data sets are used to analyze the budgets of elastic stress–velocity gradient correlations as well as Reynolds stress and dissipation transport. Closures are developed in the framework of the RSM model for all the required unknown and non-linear terms. The polymer stresses, velocity profiles, turbulent flow statistics and the percentage of friction drag reduction predicted by the RSM model are in good agreement with present and those obtained from independent DNS data over a wide range of rheological and flow parameters.

1. Introduction

The addition of a small amount of polymers to turbulent flows of Newtonian fluids can dramatically reduce the turbulent friction drag compared to that of the original Newtonian flow. It has been shown experimentally that very small amounts of polymers are sufficient to reduce drag by up to 80%. The phenomenon was found by Toms (1948) in 1949, and it has been exploited in several applications, e.g., firefighting and irrigation systems among others. Comprehensive reviews of the early literature on this topic are reported in Hoyt (1972), Lumley (1969, 1973), Virk (1975) and Virk (1971).

Two early prominent proposals by Lumley (1969) and Tabor and De Gennes (1986) describe the mechanism of turbulent drag reduction (DR) with dilute polymer solutions. Lumley proposed that flow-induced polymer stretching would increase the effective elongational viscosity in a region outside of the viscous sublayer and in the buffer layer. This in turn can inhibit turbulence-producing vortex stretching events. Tabor and De Gennes studied the drag reduction by polymer additives in the context of homogeneous isotropic turbulence, and related drag reduction to storage and release of energy by the polymer molecules.

Over the last 20 years, the development of accurate and efficient numerical and experimental methods have made it possible to investigate in detail turbulent DR of dilute polymer solutions (Poole and Escudier, 2003; Dubief et al., 2004; Ptasinski et al., 2003; Dimitropoulos et al., 2005; Li et al., 2006). Direct numerical simulations (DNSs) of turbulent channel flow of homogeneous polymer solutions have been carried out over the last two decades in order to understand various aspects of DR by investigating the effects of rheological parameters on DR mechanisms (Dimitropoulos et al., 2005; Li et al., 2006). Most of these numerical simulations have used constitutive equations based on the finitely extensible nonlinear elastic model with Peterlin's closure (FENE-P), which accounts for polymer stretching and relaxation effects as well as finite chain extensibility.

DNS of turbulent viscoelastic flow is significantly more expensive than Newtonian DNS and the CPU requirements for the DNS of viscoelastic flows are at least two orders of magnitude larger as compared to the corresponding Newtonian case, making it unfeasible for the simulation of turbulent flow in complex geometries encountered in engineering applications. Hence, Reynolds-Averaged Navier–Stokes (RANS) Poreh, 1978; Malin, 1998; Pinho, 2003; Leighton et al., 2003; Pinho et al., 2008; Resende et al., 2011, 2013; Iaccarino et al., 2010; Masoudian et al., 2013; Tsukahara and Kawaguchi, 2013, and Large Eddy Simulation (LES) models Thais et al., 2010 have been developed over the last decade.

* Corresponding author.
E-mail addresses: mmasoudian@fe.up.pt (M. Masoudian), kkim@hanbat.ac.kr (K. Kim), fpinho@fe.up.pt (F.T. Pinho), rsureshk@syr.edu (R. Sureshkumar).

http://dx.doi.org/10.1016/j.ijheatfluidflow.2015.05.017
0142-727X/

The first models for turbulent DR of polymer solutions relied on modifications of the numerical values of the coefficients for Newtonian fluid closures as done by Poreh (1978), who devised an empirical correlation to determine the constant coefficients in the standard k–ε model in order to control the behavior of the mean velocity profile in the buffer layer. Apart from the obvious consideration of lack of universality of such a closure, the major limitation is the lack of a minimal molecular representation of the behavior of the polymer solutions.

Later on, turbulence closures for non-Newtonian fluids started by modifying the von-Kármán coefficient in order to predict DR. Subsequent turbulence models were developed for inelastic fluids and included only variable viscosity effects, described by such rheological constitutive equations as the power law or Bingham law for yield stress fluids. Several first-order turbulence models were also developed for a modified version of the generalized Newtonian fluid constitutive equation in Malin (1998) and Pinho (2003) in an attempt to capture through a simple constitutive equation the effects of viscoelasticity upon turbulent friction drag.

To the best of our knowledge, the first turbulence model for turbulent flows of dilute polymer solutions described by a viscoelastic equation, such as the FENE-P model was developed by Leighton et al. (2003). In their approach, transport equations for the Reynolds and the polymer stresses were added to the mean flow equation and closures introduced to determine the unknown new correlations. Encouraging results were presented for the fully-developed flow in channel, but limited to the low drag reduction regime.

A low-Reynolds-number k–ε closure for FENE-P fluids was developed independently by Pinho et al. (2008), who relied on *a priori* analyses of DNS data. Even though the model was simpler and the Reynolds-averaged flow and conformation quantities were predicted well, the model was still limited to applications in the low DR regime (DR < 20%). Subsequently, Resende et al. (2011) developed an alternative closure for the nonlinear turbulent term of the conformation tensor equation and improved the previous closures of Pinho et al. (2008) for the viscoelastic stress work and the viscoelastic turbulent transport of the turbulent kinetic energy (k).These modifications extended the turbulence model to intermediate DR levels and in this investigation the authors also showed the limitations of a simple k–ε approach to model the flow of viscoelastic fluids. In fact, since turbulence anisotropy increases with DR, the inherent turbulence isotropy of the k–ε model leads to some conflicting variations. Hence, their model (Resende et al., 2011) is not accurate in the high DR regime. Furthermore, the model has an excessive number of damping functions and coefficients, which makes it unattractive to use, but still in a significantly less number than in Leighton et al. (2003).

Iaccarino et al. (2010) developed a k–ε–$\overline{v^2}$–f model for fully developed channel flow, which is capable of predictions over the whole range of DR. It is a fairly simple model, introducing the concept of turbulent polymer viscosity to account for the combined effects of turbulence and viscoelasticity on the polymer extra stress tensor term in the momentum equation. This turbulent polymer viscosity depends on the turbulent kinetic energy, the polymer relaxation time and the trace of the conformation tensor. Their closure of the nonlinear term in the conformation tensor equation relies on the turbulent dissipation rate. An improved k–ε–$\overline{v^2}$–f model for FENE-P fluids, developed later by Masoudian et al. (2013), is also valid up to the maximum DR and uses also the concept of turbulent polymer viscosity. It improved the prediction of the viscoelastic stress and the viscoelastic stress work, which are the main viscoelastic contributions in the momentum and the turbulent kinetic energy transport equations, respectively. Moreover, the model was tested and performed well over a wide range of rheological parameters and Reynolds numbers.

More recently, Tsukahara and Kawaguchi (2013) also proposed a low-Reynolds-number k–ε model valid up to the maximum DR, but for viscoelastic fluids described by the Giesekus constitutive equation, which is used frequently to describe the rheology of surfactant solutions. In their model, an additional damping function was introduced into the closure of eddy viscosity, while the treatment of the turbulent kinetic energy (k) and its dissipation rate (ε) is an extension of the model for Newtonian fluids.

In the present study, a new turbulence model for FENE-P fluids has been developed for the full Reynolds stress model that relies on a small number of coefficients and is capable to predict the whole range of drag reduction. An important contribution is the development of new closures for the nonlinear fluctuating terms appearing in the FENE-P rheological constitutive equation, and for the polymer stress work terms in the Reynolds stress transport equations. The model is assessed against DNS data covering a wide range of flow conditions in terms of Weissenberg number, maximum polymer extensibility (L) and Reynolds number ($Re_{\tau 0}$), and is also compared with other closures developed previously for FENE-P fluids. It is worth mentioning that only two constant coefficients were added to the original Newtonian RSM model in order to account for the influence of polymer additives on the carrier flow.

The paper is organized as follows: Section 2 introduces the instantaneous and time-averaged governing equations and identifies the viscoelastic terms requiring modeling. In Section 3, the turbulent closures are developed for the unknown terms introduced in the previous section, then Section 4 presents results of predictions for fully developed turbulent channel flow over the whole range of DR and this is followed by the conclusions.

2. Governing equations

2.1. Continuity and momentum equations

The instantaneous equations for the conservation of mass and momentum transport, appropriate for incompressible flow of FENE-P fluids are:

$$\frac{\partial \hat{u}_i}{\partial x_i} = 0 \tag{1}$$

$$\rho \frac{\partial \hat{u}_i}{\partial t} + \rho \hat{u}_k \frac{\partial \hat{u}_i}{\partial x_k} = -\frac{\partial \hat{p}}{\partial x_i} + \frac{\partial \hat{\tau}_{ik}}{\partial x_k} \tag{2}$$

where $\hat{\tau}_{ik}$ is the instantaneous stress tensor, $\hat{u}_i$ is the instantaneous velocity vector, $\hat{p}$ is the instantaneous pressure, and ρ is the fluid density. The stress tensor $\hat{\tau}_{ik}$ describes the rheology of the fluid and is given in Eq. (3) as the sum of a Newtonian solvent contribution of viscosity η_s with a polymeric contribution $\hat{\tau}_{ij,p}$ described by the FENE-P rheological constitutive model:

$$\hat{\tau}_{ij} = 2\eta_s \hat{s}_{ij} + \hat{\tau}_{ij,p} \tag{3}$$

where $\hat{s}_{ij}$ is the instantaneous rate of strain tensor defined as $\hat{s}_{ij} = \frac{1}{2}\left(\frac{\partial \hat{u}_i}{\partial x_j} + \frac{\partial \hat{u}_j}{\partial x_i}\right)$.

2.2. Constitutive equation

The instantaneous polymeric contribution to the instantaneous total extra stress is given as an explicit function of the instantaneous conformation tensor $\hat{c}_{ij}$:

$$\hat{\tau}_{ij,p} = \frac{\eta_p}{\lambda}[f(\hat{c}_{kk})\hat{c}_{ij} - f(L)\delta_{ij}] \tag{4}$$

with

$$f(\hat{c}_{kk}) = \frac{L^2 - 3}{L^2 - \hat{c}_{kk}} \quad \text{and} \quad f(L) = 1 \tag{5}$$

where $f(\hat{c}_{kk})$ is the Peterlin function, and η_p, λ and L are the rheological parameters. Specifically, they are the polymer viscosity, the relaxation time, and the maximum extension of the dumbbells, respectively. The required instantaneous conformation tensor obeys a hyperbolic differential equation of the form:

$$\left(\frac{\partial \hat{c}_{ij}}{\partial t} + \hat{u}_k \frac{\partial \hat{c}_{ij}}{\partial x_k} - \hat{c}_{jk}\frac{\partial \hat{u}_i}{\partial x_k} - \hat{c}_{ik}\frac{\partial \hat{u}_j}{\partial x_k}\right) = -\frac{\hat{\tau}_{ij,p}}{\eta_p} \tag{6}$$

The terms within the parenthesis in Eq. (6) define Oldroyd's upper convective derivative of the instantaneous conformation tensor. The first two terms represent the local and advective derivatives, which together form the material derivative, and the remaining two terms account for the distortion of c_{ij} by the flow.

2.3. DNS cases

In this study we investigate fully developed channel flow of FENE-P fluids over a wide range of conditions as described in Table 1, which lists the DNS data sets. The Reynolds number is defined as $Re_{\tau 0} \equiv hU_\tau/\nu_0$ where U_τ is the friction velocity, h is the channel half-height and ν_0 is the zero shear-rate kinematic viscosity of the solution, i.e., the sum of the kinematic viscosities of the solvent and polymer $\nu_0 = \nu_p + \nu_s$. The Weissenberg number based on the wall friction velocity is defined as $Wi_{\tau 0} \equiv \lambda U_\tau^2/\upsilon_0$ and a second Weissenberg number based on the channel half height (h) is $Wi_h \equiv \frac{Wi_{\tau 0}}{Re_{\tau 0}} = \lambda U_\tau/h$. Another relevant independent dimensionless quantity is β, the ratio between the solvent viscosity and the zero shear-rate kinematic viscosity of the solution, ($\beta \equiv \nu_s/\nu_0$). In this work, as in Sureshkumar et al. (1997) and Thais et al. (2013), a numerical diffusivity term $D\nabla^2 c$ was added to the FENE-P constitutive equation in order to perform stable numerical integration of the evolution equation for the conformation tensor, where D is a dimensionless number (equivalent to the inverse of a Schmidt number) defined as $D = \kappa/hU_\tau$, with κ denoting a constant isotropic artificial numerical diffusivity. The diffusivity is chosen in a way that it is large enough for the calculations to ensure the numerical stability of the calculations and the realizability of the conformation tensor values, while small enough that it does not affect the computational results. This follows on the steps of Sureshkumar et al. (1997) and the normalized artificial numerical diffusivity D was taken to be of $O(10^{-2})$ resulting in a numerical Schmidt number $Sc^+ = 1/Re_{\tau 0}D$ of the order $O(10^{-1})$.

Periodic boundary conditions were applied along the streamwise and spanwise directions. The channel size was chosen to adequately capture the streaky structures and the elongated vortical structures developed in the flow. In the two periodic directions, *x and z*, Fourier representations were used, whereas in the non-homogeneous shear direction a Chebyshev approximation was employed. As shown above, the flow and polymer stress fields can be fully characterized by dimensionless groups, namely, Re_τ, β, L^2 and Wi_h (or $Wi_{\tau 0}$). Further details of the numerical approaches used in this work can be found in Li et al. (2006). Table 1 summarizes the computational parameters for the DNSs performed in the present study. Fig. 1 shows the profiles of streamwise mean velocity and root mean square of the velocity fluctuations for DNS3 and DNS4 cases, which corresponds to low and high DR regimes, respectively. The present DNS results are in an excellent agreement with previous DNS data (Li et al., 2006). Note that, as demonstrated in Li et al. (2006), for low drag reduction the temporal averaging is performed over 10–15 computational units (h/U_τ), whereas much longer temporal averaging period over 30–50 h/U_τ is required to obtain converged statistics for high DR flows due to the significant variations in xz plane. Although this approach ensures the time averaged statistics to remain stationary, an uncertainty analysis can be performed in future to assess the DNS data of turbulent polymer dilute solution as was carried out recently to analyze DNS of Newtonian channel flow by Oliver et al. (2014).

2.4. Reynolds-averaged equations

In Reynolds-averaged methods the instantaneous quantities are decomposed into the sum of a mean value and a fluctuating value as in $\hat{u}_i = U_i + u_i$, $\hat{p} = P + p$, and $\hat{c}_{ij} = C_{ij} + c_{ij}$, where upper-case letters or overbars denote Reynolds-averaged quantities and lower-case letters or primes denote fluctuating quantities. A hat denotes an instantaneous quantity. The Reynolds-averaged equations appropriate for incompressible flow of FENE-P fluids are the continuity equation:

$$\frac{\partial U_i}{\partial x_i} = 0 \tag{7}$$

and the momentum equation

$$\rho\frac{\partial U_i}{\partial t} + \rho U_k \frac{\partial U_i}{\partial x_k} = -\frac{\partial \overline{P}}{\partial x_i} + \rho\frac{\partial}{\partial x_k}(-\overline{u_i u_k}) + \frac{\partial \bar{\tau}_{ik}}{\partial x_k} \tag{8}$$

where $\bar{\tau}_{ik}$ is the Reynolds-averaged stress tensor, U_i is the mean velocity, $\overline{P}$ is the mean pressure, $-\overline{u_i u_k}$ is the Reynolds stress tensor, and $\bar{\tau}_{ik}$ is the Reynolds averaged fluid extra stress tensor. In the Reynolds-averaged Navier–Stokes (RANS) equation (Eq. (8)) the Reynolds stress tensor ($-\overline{u_i u_k}$) is unknown, and needs a closure. The full RSM turbulence model is used to determine the Reynolds stresses. An exact transport equation for the Reynolds stresses can be derived from the Navier–Stokes equation for FENE-P fluids.

Table 1
Summary of the physical and computational parameters for the DNS cases used in this work.

Case	$Re_{\tau 0}$	Domain size ($L_x \times L_y \times L_z$)	Grid (n_x, n_y, n_z)	L^2	$Wi_{\tau 0}$	Wi_h	β
DNS0	180	6.283 h × 2 h × 3.141 h	128 × 129 × 128	0	0	0	0
DNS1	395	14.136 h × 2 h × 4.5 h	384 × 257 × 192	0	0	0	0
DNS2	590	14.136 h × 2 h × 4.5 h	512 × 257 × 256	0	0	0	0
DNS3	180	6.944 h × 2 h × 4.19 h	128 × 129 × 128	900	25	0.139	0.9
DNS4	180	6.944 h × 2 h × 4.19 h	128 × 129 × 128	3600	100	0.55	0.9
DNS5	395	14.136 h × 2 h × 4.5 h	512 × 129 × 192	900	25	0.063	0.9
DNS6	395	14.136 h × 2 h × 4.5 h	384 × 257 × 192	900	75	0.19	0.9
DNS7	395	14.136 h × 2 h × 4.5 h	384 × 257 × 192	3600	75	0.19	0.9
DNS8	395	14.136 h × 2 h × 4.5 h	384 × 257 × 192	14,400	75	0.19	0.9
DNS9	395	14.136 h × 2 h × 4.5 h	384 × 257 × 192	3600	100	0.25	0.9
DNS10	395	14.136 h × 2 h × 4.5 h	384 × 257 × 192	3600	50	0.125	0.9
DNS11	590	25.136 h × 2 h × 4.5 h	512 × 257 × 256	3600	50	0.085	0.9
DNS12	590	25.136 h × 2 h × 4.5 h	512 × 257 × 256	10,000	100	0.17	0.9

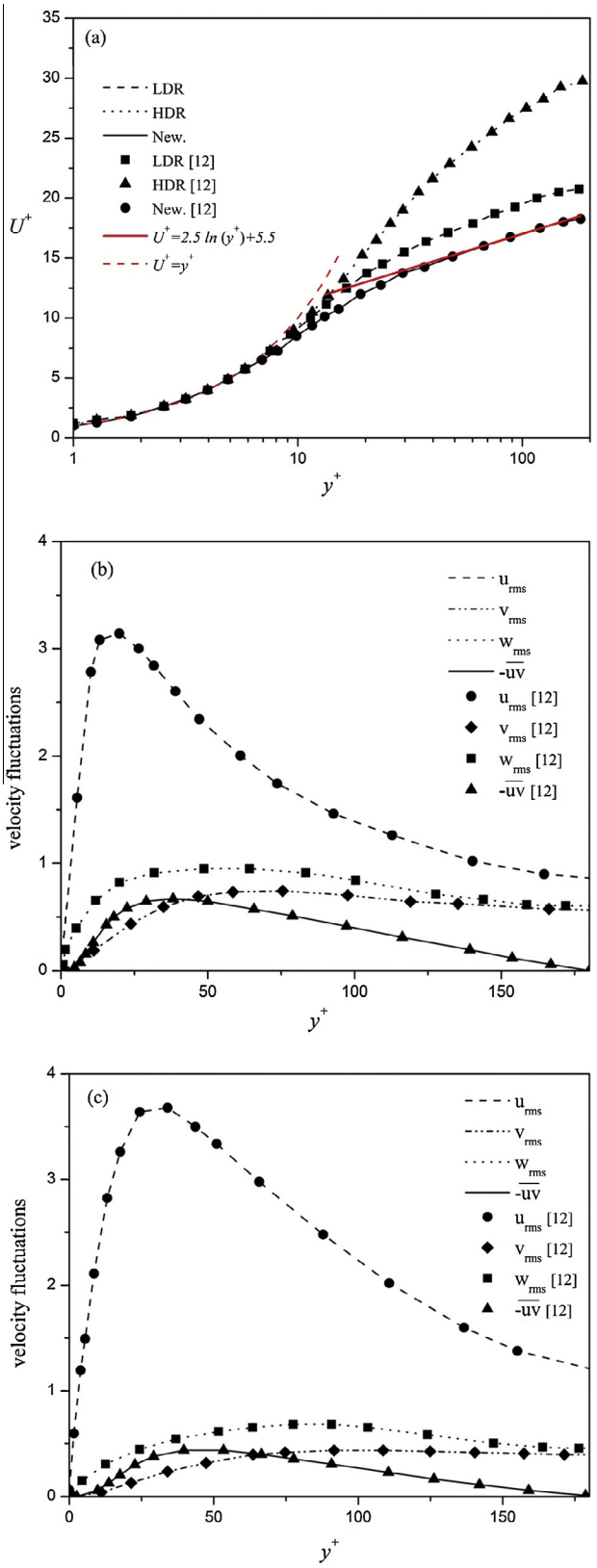

Fig. 1. Comparison of current DNS results for LDR and HDR (cases DNS3, and DNS4 Table 1) with DNS results of Li et al. (2006), (a) mean streamwise velocity profiles, (b) rms of velocity fluctuations and Reynolds stress for LDR case, and (c) rms of velocity fluctuations and Reynolds stress for HDR case.

It is emphasized that this equation is exact or rather as exact as the Navier–Stokes equations. The Reynolds stress transport equation appropriate for FENE-P fluids can be written as:

$$\frac{\partial \overline{u_i u_j}}{\partial t}+U_k\frac{\partial \overline{u_i u_j}}{\partial x_k}=\underbrace{\left(-\overline{u_i u_k}\frac{\partial U_j}{\partial x_k}-\overline{u_j u_k}\frac{\partial U_i}{\partial x_k}\right)}_{P_{ij}}+\underbrace{\frac{\partial}{\partial x_k}\left(\nu\frac{\partial \overline{u_i u_j}}{\partial x_k}\right)}_{D_{ij,\nu}}$$
$$\underbrace{-\frac{\partial}{\partial x_k}\left(\overline{u_i u_j u_k}+\overline{\frac{p}{\rho}(\delta_{jk}u_i+\delta_{ik}u_j)}\right)}_{D_{ij,t}}$$
$$\underbrace{-2\nu\overline{\frac{\partial u_i}{\partial x_k}\frac{\partial u_j}{\partial x_k}}}_{\varepsilon_{ij}}+\underbrace{\overline{\frac{p}{\rho}\left(\frac{\partial u_i}{\partial x_j}+\frac{\partial u_j}{\partial x_i}\right)}}_{\Pi_{ij}}+\underbrace{\frac{\partial}{\partial x_k}\left(\overline{u_i\tau_{jk,p}+u_j\tau_{ik,p}}\right)}_{D_{ij,p}}$$
$$\underbrace{-\overline{\left(\tau_{ik,p}\frac{\partial u_j}{\partial x_k}+\tau_{jk,p}\frac{\partial u_i}{\partial x_k}\right)}}_{\varepsilon_{ij,p}} \tag{9}$$

Except for the last two terms on the right-hand-side, which involve the fluctuating polymer stresses, the other terms are classical terms appearing in the corresponding equation for Newtonian fluids and represent the turbulence production by the mean strain (P_{ij}), molecular diffusion ($D_{ij,\nu}$), turbulent transport ($D_{ij,t}$), viscous dissipation by the solvent (ε_{ij}) and the pressure–strain term (Π_{ij}). The last two terms on the right-hand-side are viscoelastic terms representing the viscoelastic turbulent transport ($D_{ij,p}$) and the viscoelastic stress work ($\varepsilon_{ij,p}$). In order to have an idea about the magnitude of the different terms in the Reynolds stress transport equation, the budgets of Eq. (9) for all components of the Reynolds stress tensor are plotted in Fig. 2 for the data set DNS5. These data are presented in dimensionless form utilizing all turbulent scales and in order to normalize data the quantities υ/U_τ and υ/U_τ^2 are used as the length and time scales, respectively.

As it can be seen in Fig. 2(a) the viscoelastic stress work is negative all across the channel meaning that it behaves as a sink in the transport of the streamwise Reynolds stress. Fig. 2(a) also shows that although the viscoelastic stress work is small close to the wall, when compared with the other terms, far from the wall it has the same magnitude as the production and the solvent dissipation terms. Moreover, Fig. 2(a) shows that the viscoelastic turbulent transport has a small magnitude near the wall, and it is almost zero away from the wall. Budgets of Reynolds stress terms in the wall-normal and spanwise directions are plotted in Fig. 2(b) and (c), respectively. As expected the pressure strain term is the most important positive term in these directions, where it plays a pseudo-production role in its quantification of the transfer of energy from the streamwise direction. Viscoelastic stress work, on the other hand, is negative and behaves as a sink of energy, as in the streamwise direction. The figure also shows that for the $\overline{v'v'}$ and $\overline{w'w'}$ components the viscoelastic stress work has the same magnitude as the pressure strain and the viscous dissipation terms all across the channel. Moreover, as in the streamwise direction, the viscoelastic turbulent transport is very small and active only close to the wall. Fig. 2(d) shows the budget of the Reynolds shear stress (xy component) and, as expected, the viscoelastic stress work, the viscous dissipation by the solvent, and the pressure strain terms all have the same sign all across the channel. Moreover, the viscoelastic stress work has the same intensity as the viscous dissipation by the solvent, whereas the viscoelastic turbulent transport is negligible as was the case previously for the normal components.

The Reynolds-averaged total extra stress tensor $\bar{\tau}_{ij}$ can be calculated by Reynolds averaging Eq. (3) leading to

$$\bar{\tau}_{ij}=2\eta_s S_{ij}+\bar{\tau}_{ij,p} \tag{10}$$

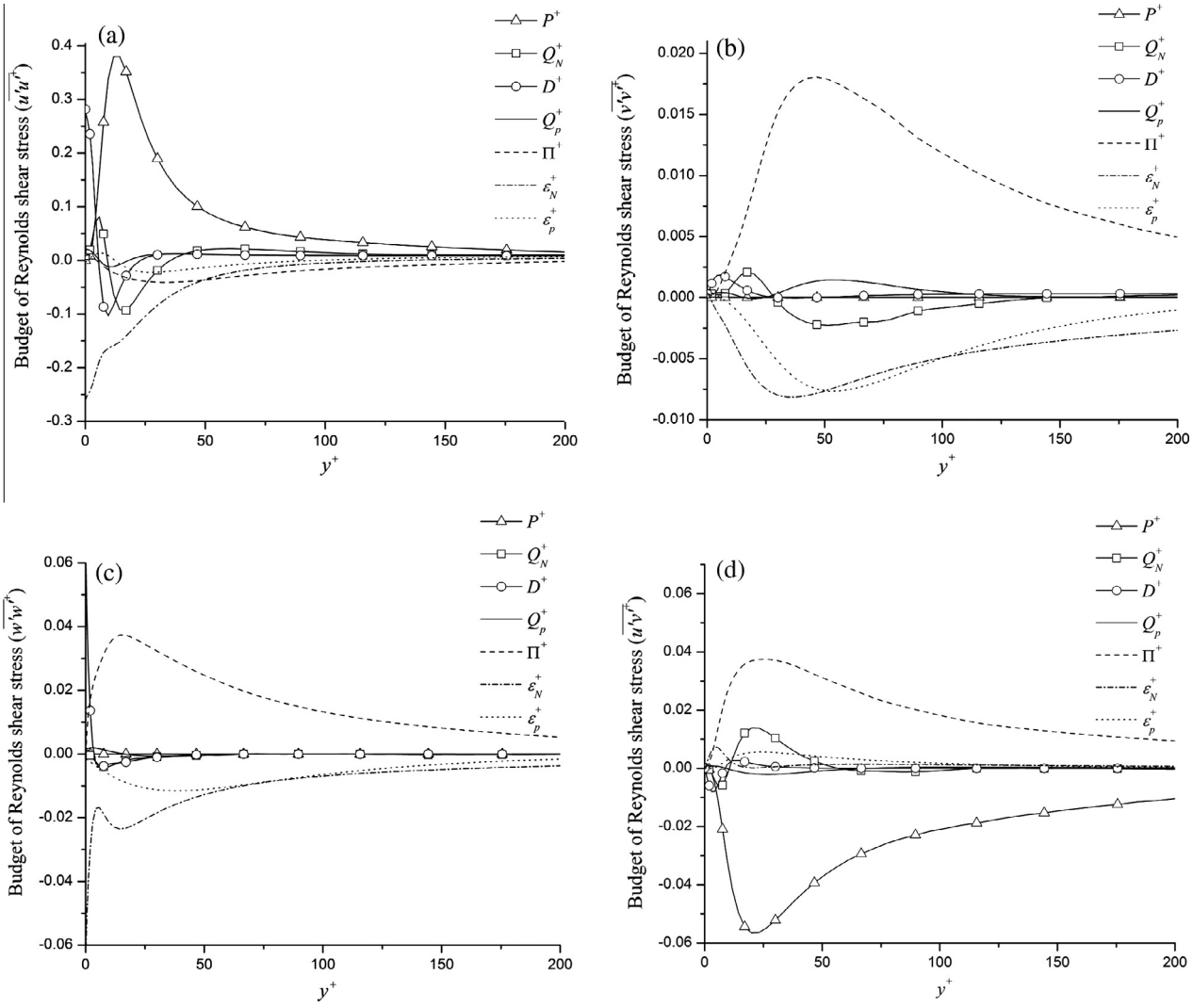

Fig. 2. Budgets of components of Reynolds stress transport equation for the flow of FENE-P fluids for case DNS5 ($Re_{\tau 0}$ = 395, $Wi_{\tau 0}$ = 25 and L^2 = 900), (a) $\overline{u'u'}$, (b) $\overline{v'v'}$, (c) $\overline{w'w'}$, and (d) $\overline{u'v'}$.

where S_{ij} is the mean rate of strain tensor. Then, by Reynolds-averaging Eq. (4), the Reynolds-averaged polymer stress $\bar{\tau}_{ij,p}$ is given by:

$$\bar{\tau}_{ij,p} = \frac{\eta_p}{\lambda}\left[f(C_{kk})C_{ij} - f(L)\delta_{ij}\right] + \frac{\eta_p}{\lambda}\left[\overline{f(C_{kk}+c_{kk})(C_{ij}+c_{ij})} - f(C_{kk})C_{ij}\right] \quad (11)$$

Eq. (11) depends on the time-averaged form of the conformation tensor, which must be determined from the corresponding time averaged evolution equation, given as:

$$\overset{\nabla}{C}_{ij} + \overline{u_k\frac{\partial c_{ij}}{\partial x_k}} = \left(\overline{c_{jk}\frac{\partial u_i}{\partial x_k}} + \overline{c_{ik}\frac{\partial u_j}{\partial x_k}}\right) - \frac{\bar{\tau}_{ij,p}}{\eta_p} \quad (12)$$

After substitution of Eq. (11), and expanding $\overset{\nabla}{C}_{ij}$, Eq. (12) becomes:

$$\left(U_k\frac{\partial C_{ij}}{\partial x_k} - \underbrace{\left(C_{jk}\frac{\partial U_i}{\partial x_k} + C_{ik}\frac{\partial U_j}{\partial x_k}\right)}_{M_{ij}}\right) + \left(\underbrace{\left(\overline{u_k\frac{\partial c_{ij}}{\partial x_k}}\right)}_{CT_{ij}} - \underbrace{\left(\overline{c_{jk}\frac{\partial u_i}{\partial x_k}} + \overline{c_{ik}\frac{\partial u_j}{\partial x_k}}\right)}_{NLT_{ij}}\right)$$
$$= -\frac{1}{\lambda}\left[f(C_{kk})C_{ij} - f(L)\delta_{ij}\right] - \frac{1}{\lambda}\left[\overline{f(C_{kk}+c_{kk})(C_{ij}+c_{ij})} - f(C_{kk})C_{ij}\right] \quad (13)$$

On the left-hand-side of Eq. (13), the mean flow advective term vanishes for fully developed channel flow. The mean flow distortion term of $\overset{\nabla}{C}_{ij}$ is M_{ij} and the remaining two terms on the left-had-side of Eq. (13) correlate fluctuating velocities and conformation tensor components. Term CT_{ij} represents the contribution of the fluctuating velocity field to the advective transport of the mean conformation tensor. The interaction between the fluctuating components of the conformation tensor and of the velocity gradient tensor, originating from the Oldroyd derivative, is denoted by NLT_{ij} and is the fluctuating counterpart of M_{ij}. In the Reynolds-averaged constitutive equation (Eq. (13)) the mean flow distortion term (M_{ij}) needs no closure. The advective transport of the conformation tensor (CT_{ij}) and the fluctuating polymer stretching terms (NLT_{ij}), which account for the fluctuating counterpart of M_{ij} are both non-linear and developing closures for them will be one of the main tasks of this work. Finally, a closure is also needed for the last term on the right-hand-side of Eq. (13).

To ascertain the contributions of different terms in Eq. (13), the components of the M_{ij}, NLT_{ij}, and CT_{ij} tensors are plotted in Fig. 3 in all directions. As expected, the mean flow distortion term of $\overset{\nabla}{C}_{ij}$, M_{ij}, is the most important term close to the wall in the evolution

equation for the transport of C_{xx}, then it decays with wall distance, whereas NLT_{xx} increases from zero at the wall and becomes the main contributor in the buffer layer. It is clear from Fig. 3(a) that in the log-law region both M_{xx} and NLT_{xx} have similar magnitudes. In contrast CT_{xx} is very small in comparison with both M_{xx}, and NLT_{xx} all across the channel. For the shear component shown in Fig. 3(b), the shape of the curves is somewhat different, but again the main contributions come from NLT_{xy}, and M_{xy}. Likewise the streamwise direction, CT_{xy} is negligible. For the remaining two normal directions, as shown in Fig. 3(c) and (d) the mean flow distortion term is null, hence NLT_{yy}, and NLT_{zz} provide the main contribution for the y and z component equations, respectively. In contrast, both CT_{yy} and CT_{zz} are again small and negligible for each of the corresponding balances. The obvious conclusion is that a closure must be developed for NLT_{ij}, but CT_{ij} can simply be ignored. Note that, this simplification is tested for all the cases described in Table 1 to ensure that CT_{ij} has negligible magnitude regardless of the flow and rheological parameters. Similarly to the low DR flow, Fig. 4 shows that CT_{ij} is much smaller than NLT_{ij} and M_{ij} terms for high DR flows (DNS9). It was found that for all DNS cases CT_{ij} is less than 5% of the main contributors i.e., NLT_{ij}, and M_{ij}. For the sake of comparison this term plotted along with NLT_{ij} and M_{ij} terms for the high drag reduction case (DNS9) in Fig. 4 confirming that this assumption is correct. It is worth mentioning that a similar conclusion had already been reached in Masoudian et al. (2013) in the context of k–ε–$\overline{v^2}$–f.

3. Development of closures

In this section closures are developed for all non-negligible unknown turbulent cross-correlations in the various governing equations. The terms requiring closures in the time-averaged constitutive equation are the second term on the right-hand-side of the time-averaged polymer stress (Eq. (11)), and the cross-correlation between the fluctuating components of the conformation tensor and of the velocity gradient tensor, $NLT_{ij} = \overline{c_{jk}\partial u_i/\partial x_k} + \overline{c_{ik}\partial u_j/\partial x_k}$. In addition, closures must be developed for the nonlinear viscoelastic terms appearing in the transport equation for the Reynolds-averaged stress tensor, the last two terms on the left hand side of Eq. (9), namely the viscoelastic turbulent transport ($D_{ij,p}$) and the viscoelastic stress work ($\varepsilon_{ij,p}$).

3.1. A model for the constitutive equation

As described in the previous section the first term that needs to be calculated is the time-averaged polymer stress, Eq. (11). In this

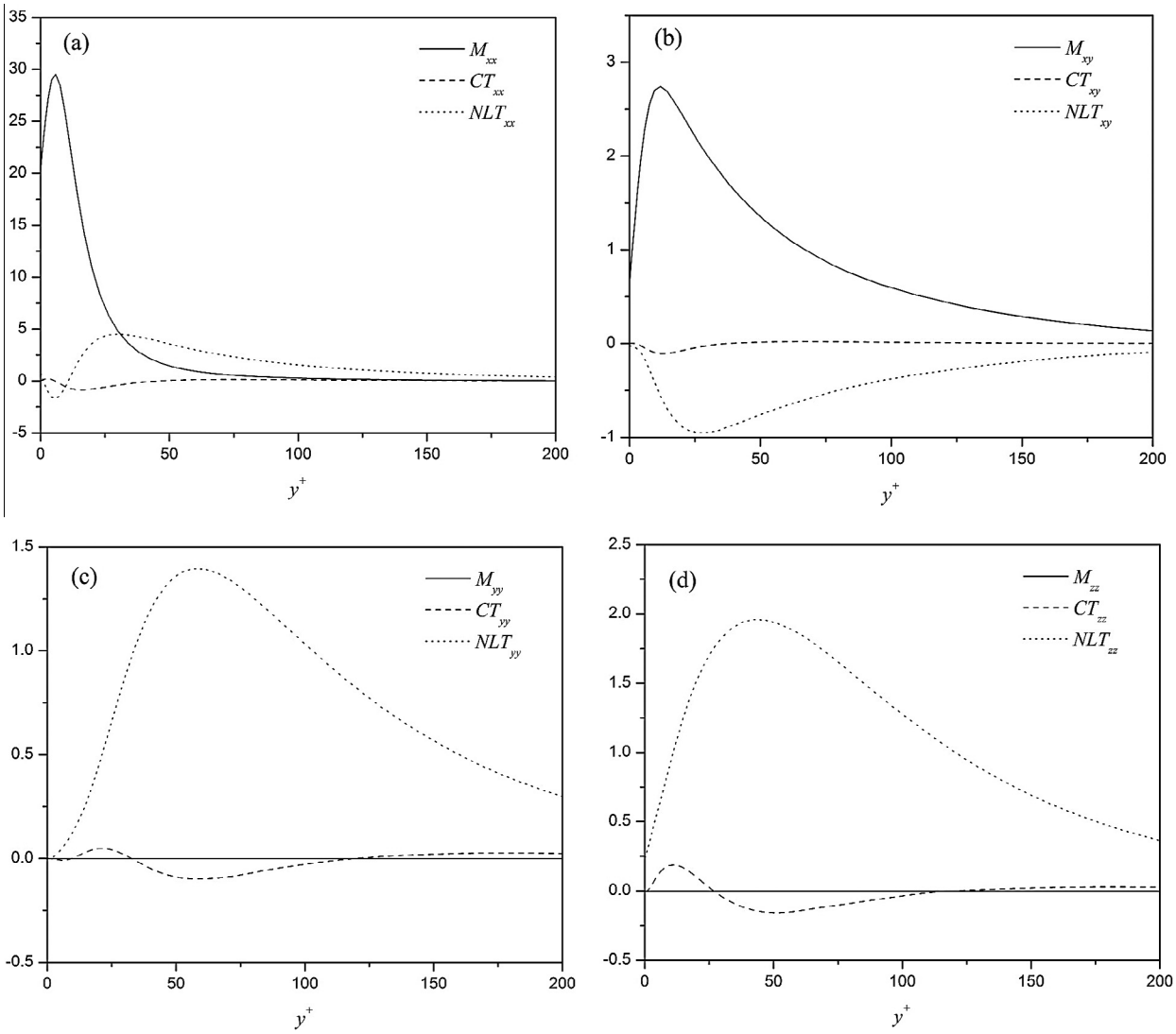

Fig. 3. Variation across the channel of components M_{ij}, NLT_{ij}, and CT_{ij} for case DNS5, $Re_{\tau 0} = 395$, $Wi_{\tau 0} = 25$ and $L^2 = 900$, (a) xx-component, (b) xy-component, (c) yy-component, and (d) zz-component.

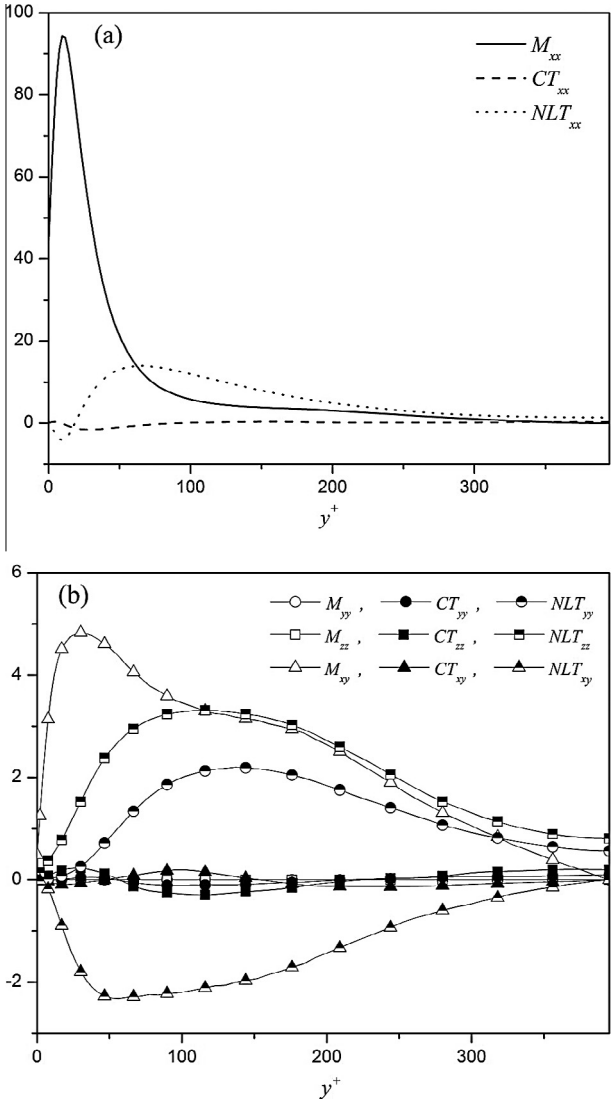

Fig. 4. Variation across the channel of components M_{ij}, NLT_{ij}, and CT_{ij} for high drag reduction case DNS9, $Re_{\tau 0} = 395$, $Wi_{\tau 0} = 100$ and $L^2 = 3600$, (a) *xx*-component, and (b) *xy*, *yy*, *zz*-components.

work $\bar{\tau}_{ij,p}$ is approximated as the first term on the right hand side of Eq. (11), i.e., the second term is neglected, because both terms on the right-hand-side of Eq. (11) were compared in Iaccarino et al. (2010) and Masoudian et al. (2013) by using *a priori* DNS data at different values of $Wi_{\tau 0}$ and L^2, and it was shown that the first exact term is nearly 20 times larger than the second term regardless of the amount of drag reduction. Consequently by using this assumption the Reynolds-averaged polymer stress will be calculated by using only the first term as:

$$\bar{\tau}_{ij,p} = \frac{\eta_p}{\lambda}\left[f(C_{kk})C_{ij} - f(L)\delta_{ij}\right] \tag{14}$$

As described in the previous section, NLT_{ij} plays an important role in the Reynolds-averaged conformation tensor equation, and its closure constitutes a major task in this work. Apart from NLT_{ij}, the other main contribution to the Reynolds-averaged conformation tensor equation comes from the exact mean flow term (M_{ij}), especially close to the wall. In the context of k–ε–$\overline{v^2}$–f models Iaccarino et al. (2010) and Masoudian et al. (2013) proposed closures for the trace of NLT_{ij}, but since in this work a full RSM model is being developed all components of NLT_{ij} need closure.

Using the DNS data all components of the mean polymer conformation tensor, C_{ij}, are plotted in the various parts of Fig. 5. In addition, the polymer conformation that would result only from the mean flow distortion term (M_{ij}) is calculated and plotted in Fig. 5 as C_{ij}^M. This is equivalent to considering Eq. (13) as if M_{ij} was the single existing term and NLT_{ij} was zero. Due to the elimination of CT_{ij} from Eq. (13), because of its negligible magnitude for all components, the difference between those two quantities, $C_{ij}^{NLT} = C_{ij} - C_{ij}^M$, corresponds to the effect of NLT_{ij} upon polymer elongation and orientation, which we refer to as the turbulent polymer conformation difference. Fig. 5 shows that the turbulent polymer conformation difference exhibits qualitatively a very similar behavior to the time-averaged Reynolds stress components in terms of peak location, overall sign and shape (note the different ordinate axis). The correlation between NLT_{kk} term and the turbulent kinetic energy was introduced by Iaccarino et al. (2010) in the context of k–ε–$\overline{v^2}$–f, and here we are adapting and generalizing the same concept to the RS model by introducing a direct relation between NLT_{ij} and the Reynolds stress tensor.

In order to have an idea about instantaneous fields, iso-surfaces of instantaneous "Reynolds stress" components and instantaneous NLT_{ij} components are plotted for case DNS3 in Fig. 6. It is interesting to note that instantaneous $\widehat{NLT}_{ij}$ and u_iu_j events usually occur in close proximity to each other, and as it can be seen the $\widehat{NLT}_{ij}$ events being generally surrounded by a region of significant u_iu_j events. In physical terms the polymer elongation and orientation due to the NLT_{ij} contribution represents the ability of the turbulent fluctuations to act on the polymer chains. In summary, the DNS data analysis of all cases described in Table 1 shows a direct relation between the components of the averaged Reynolds stress tensor and the NLT_{ij} tensor on a component to component basis, both near and far from the wall, i.e., $NLT_{ij} \propto \overline{u_iu_j}$. Moreover the stretching of the polymers can be effective only if the turbulent time scale is short enough with respect to the relaxation time, therefore the ratio of the polymer relaxation time, λ, to the turbulent time scale, $T_t = k/\varepsilon$, must be added to the closure.

Furthermore, analyzing the current DNS data sets together with the independent DNS results of Thais et al. (2013) at different Reynolds numbers shows that NLT_{ij} has a direct relation with the polymer maximum extension. Hence, the quantity $Wi_h\sqrt{L}/(\upsilon_p f(C_{kk}))$ and the coefficient a_1 were added to the closure of NLT_{ij} after running an optimization algorithm to quantify the coefficient for optimum model performance. The final form of the closure for NLT_{ij} is:

$$NLT_{ij} = a_1 \frac{\lambda}{\upsilon_p}\frac{\varepsilon}{k}\frac{Wi_h\sqrt{L}}{f(C_{kk})}\overline{u_iu_j} \tag{15}$$

Note that the product $\lambda\ \overline{u_iu_j}$ in Eq. (15) has the dimensions of a diffusivity and can be interpreted as a turbulent viscoelastic viscosity, $\upsilon_{T,p}$. Conceptually, this is in agreement with the previous closures developed in Iaccarino et al. (2010) and Masoudian et al. (2013) for NLT_{kk} in the context of k–ε–$\overline{v^2}$–f turbulence models.

3.2. Closures required for the Reynolds stress transport equation

In this work we use the Reynolds stress (RS) model developed by Lai and So (1990) for Newtonian fluids as the base model to develop the modified RS model for FENE-P fluids. The terms on the left-hand side of the exact Reynolds stress transport equation (Eq. (9)) concern the time variation, and the advection of the Reynolds stress. These are exact terms that do not require modeling. The first two terms on the right-hand-side of Eq. (9), representing the production and the molecular diffusion of the Reynolds stress, are also exact are do not require a closure, whereas the

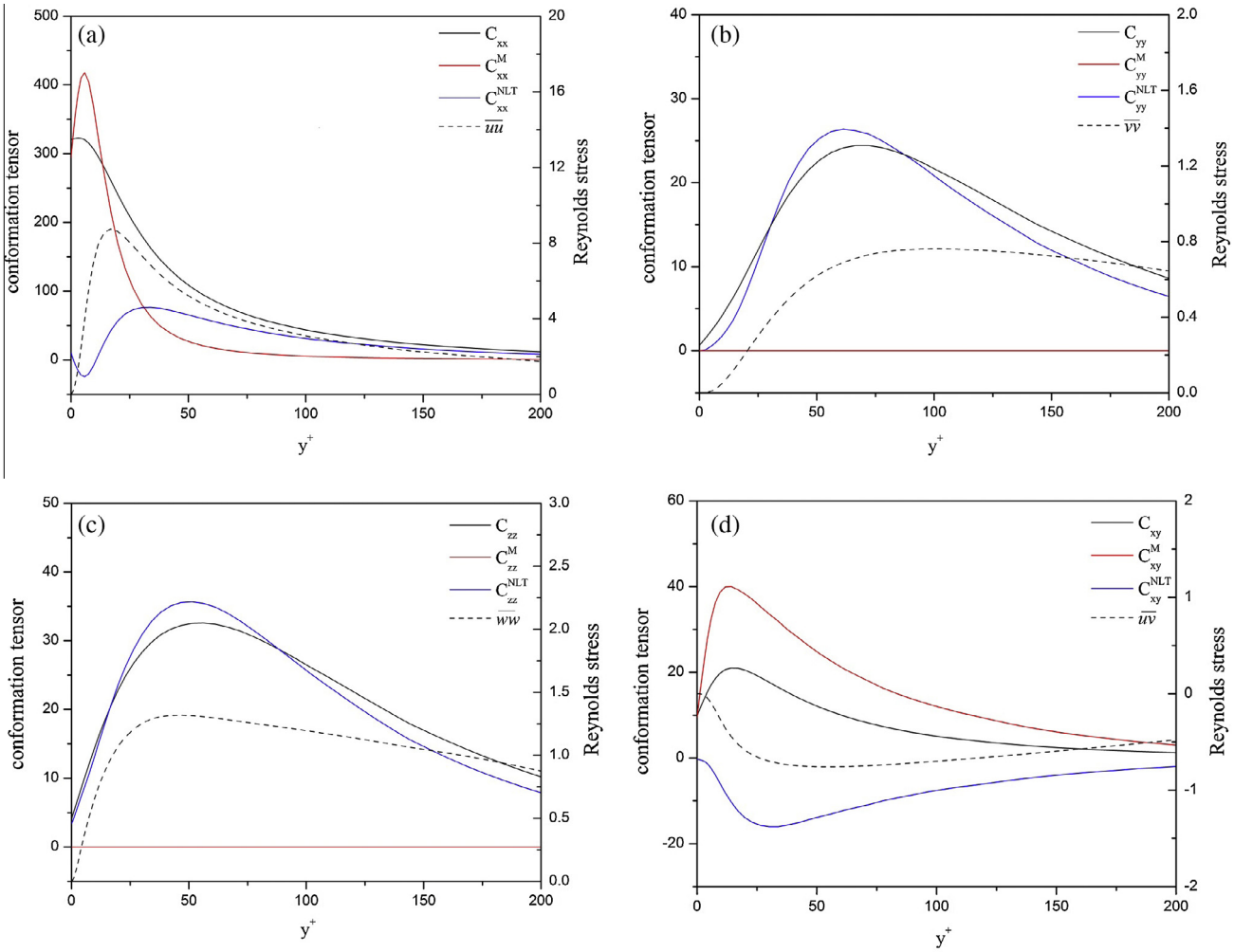

Fig. 5. Profiles of C_{ij}, C_{ij}^{M}, C_{ij}^{NLT}, and $\overline{u_i'u_j'}$ for case DNS5, $Re_{\tau 0} = 395$, $Wi_{\tau 0} = 25$ and $L^2 = 900$, (a) *xx*-component, (b) *yy*-component, (c) *zz*-component, and (d) *xy*-component.

remaining terms need to be modeled. Except for the last two terms, which are the viscoelastic contributions, all other terms in the Reynolds stress transport equation are identical to those in the corresponding equation for Newtonian fluids. The first term that needs closure is the turbulent transport ($D_{ij,t}$), consisting of the turbulent diffusion by velocity fluctuations and the turbulent diffusion by pressure fluctuations. Usually the turbulent diffusion by pressure is neglected at high Reynolds number flows or incorporated as part of the turbulent diffusion by velocity fluctuations (Lai and So, 1990). In the budget of the Reynolds stress equation for FENE-P fluids the turbulent diffusion is small and behaves similarly to the corresponding term for Newtonian fluids, consequently in this work we use the Newtonian closure of Lai and So (1990) to model turbulent diffusion for viscoelastic fluids as:

$$D_{ij,t} = \rho \frac{\partial}{\partial x_k}\left(C_s \frac{k}{\varepsilon}\left[\overline{u_i u_l}\frac{\partial \overline{u_j u_k}}{\partial x_l} + \overline{u_j u_l}\frac{\partial \overline{u_k u_i}}{\partial x_l} + \overline{u_k u_l}\frac{\partial \overline{u_i u_j}}{\partial x_l}\right]\right) \tag{16}$$

The second classical term that needs closure is the viscous dissipation by the solvent (ε_{ij}), here modeled as by Lai and So (1990) in Eq. (17) (note that this closure was initially developed by Shima (1988).

$$\varepsilon_{ij} = \frac{2}{3}\varepsilon(1-f_w)\delta_{ij} + \frac{f_w(\varepsilon/k)\left[\overline{u_i u_j} + \overline{u_i u_k}n_k n_j + \overline{u_j u_k}n_k n_i + n_i n_j \overline{u_k u_l}n_k n_l\right]}{1 + 3\overline{u_k u_l}n_l n_k/2k}, \tag{17}$$

where n_i denotes the wall unit normal vector. The rate of dissipation tensor ε_{ij} relies on the isotropic scalar rate of dissipation of turbulent kinetic energy (ε), which is calculated by its own transport equation:

$$\frac{D\varepsilon}{Dt} = \frac{\partial}{\partial x_k}\left(\upsilon\frac{\partial \varepsilon}{\partial x_k}\right) + \frac{\partial}{\partial x_k}\left(C_s\frac{k}{\varepsilon}\overline{u_k u_i}\frac{\partial \varepsilon}{\partial x_i}\right) + C_{\varepsilon 1}(1+\sigma f_{w,2})\frac{\varepsilon}{k}\widetilde{P} - C_{\varepsilon 2}f_\varepsilon\frac{\varepsilon\tilde{\varepsilon}}{k} + f_{w,2}\left[\left(\frac{7}{9}C_{\varepsilon 2}-2\right)\frac{\varepsilon\tilde{\varepsilon}}{k} - \frac{1}{2k}\left(\varepsilon - \frac{2\upsilon k}{y^2}\right)^2\right] - E_p \tag{18}$$

where the pseudo-dissipation ($\tilde{\varepsilon}$) and $\widetilde{P}$ appearing in Eq. (18) are given by:

$$\tilde{\varepsilon} = \varepsilon - 2\upsilon\left(\frac{\partial k^{0.5}}{\partial y}\right)^2$$

$$\widetilde{P} = 0.5P_{ii}, \quad P_{ii} = \overline{u_i u_k}\frac{\partial U_j}{\partial x_k} + \overline{u_j u_k}\frac{\partial U_i}{\partial x_k}$$

In Eq. (18), all terms are conceptually identical to those for a Newtonian fluid except for the last term (E_p) representing the viscoelastic contribution to the transport equation of ε. In this work as in Masoudian et al. (2013) E_p is assumed to be a destruction term of ε, and we use the closure given by Masoudian et al. (2013) as:

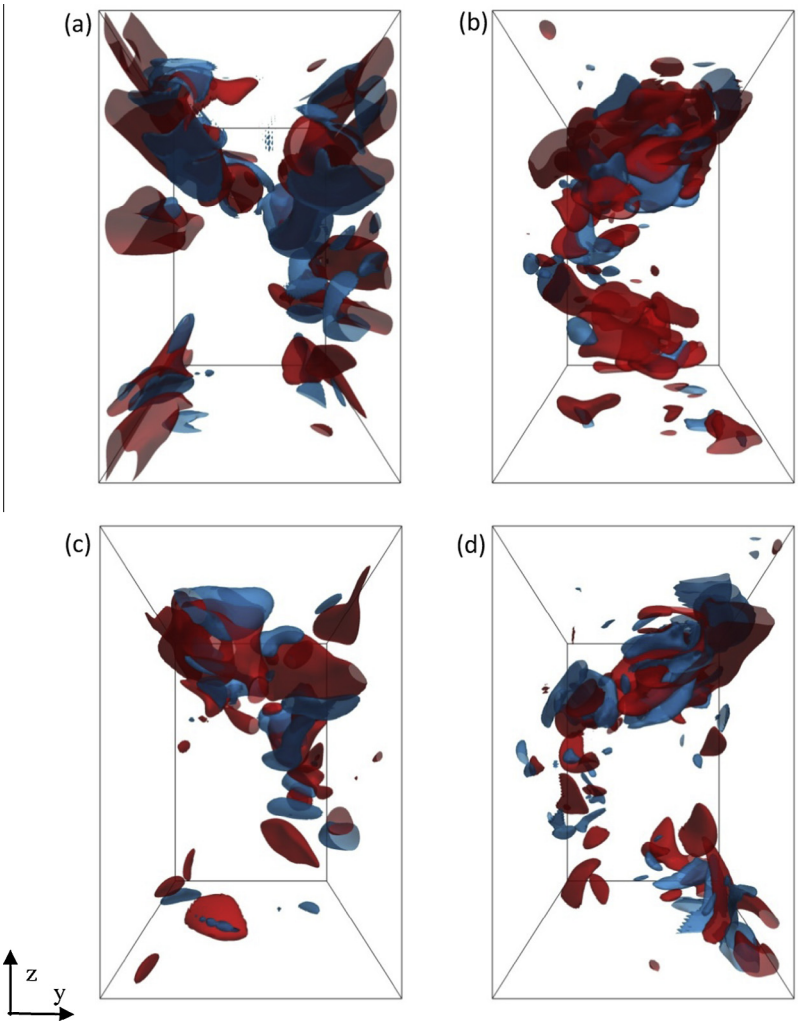

Fig. 6. Visualizations of iso-surfaces of instantaneous fields of the "Reynolds stress" (u_iu_j) components (Red) and $\widehat{NLT}_{ij}$ components (Blue) using DNS3 case. Figures show y–z plane, and iso-surfaces were made transparent (70% opacity) to help visualizations. The threshold for all quantities is 10% of the maximum value of each quantity. (a) $\widehat{NLT}_{xx}$, u_xu_x, (b) $\widehat{NLT}_{yy}$, u_yu_y, (c) $\widehat{NLT}_{zz}$, u_zu_z, and (d) $\widehat{NLT}_{xy}$, u_xu_y. (For interpretation of the references to color in this figure legend, the reader is referred to the web version of this article.)

$$E_p = a_2 \varepsilon_{ii,p} \frac{\varepsilon}{k} \tag{19}$$

The predicted dissipation rate using the present model is compared with the DNS data in Fig. 7. The present model prediction of ε^+ is in good agreement with DNS data, which can be attributed to the use of the model of Masoudian et al. (2013) that is capable of predicting the scalar rate of turbulent dissipation both close and far from the wall.

The pressure–strain term is important in the budgets of the normal components of the Reynolds stress tensor, especially in the wall-normal and spanwise directions. It distributes the turbulent kinetic energy across the components, namely extracting the energy from the streamwise component to inject it into the two cross-stream components. As for the Newtonian case the pressure strain for the streamwise component is negative (sink) and by adding polymer, based on the numerical and experimental findings of Ptasinski et al. (2003) and Li et al. (2006), its peak value decreases and moves away from the wall. Similar variations are observed for the pressure strain terms in the wall-normal and spanwise components, except that the quantities are now positive (source). This is consistent with the lower levels of v_{rms} and w_{rms} observed experimentally and numerically in drag-reduced flows by polymer additives in comparison to the corresponding values for Newtonian flows. Due to the importance of the pressure strain especially in the wall-normal and spanwise directions, predicted pressure strain terms for all components are plotted in Fig. 8 using the original closure developed for Newtonian fluids by Lai and So. As it can be seen the Newtonian closure is capable of predicting the suppression of pressure strain term typically observed with polymer solutions without need for any closure modification. And as we will see in the results section the predictions of the wall normal and spanwise turbulent intensities, in which the pressure strain term is the most important source term, are in perfect agreement with DNS data using the Newtonian pressure strain closure. It is worth mentioning that Iaccarino et al. (2010) and Masoudian et al. (2013) examined different closures to account for the reduction of the pressure strain term of the wall-normal component of Reynolds stress in the context of k–ε–$\overline{v^2}$–f and they found that incorporation of corrections to the pressure strain term caused complete flow laminarization and numerical divergence at high drag reduction, very much as we found here in the context of the full second order Reynolds stress model. As a result the pressure strain term for viscoelastic fluid flows is here calculated by the Newtonian closure of Lai and So (1990) as:

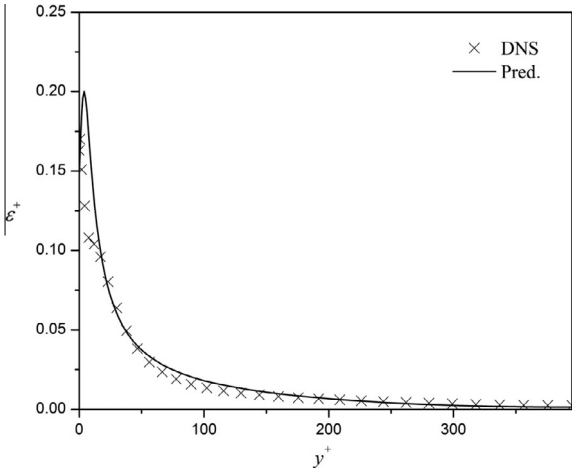

Fig. 7. Prediction of dissipation of turbulent kinetic energy using Eq. (19). $Re_\tau = 395$, $Wi_\tau = 25$ and $L^2 = 900$.

$$\Pi_{ij} = \Pi_{ij,1} + \Pi_{ij,w} f_{w1}$$
$$\Pi_{ij,1} = -C_1 \frac{\varepsilon}{k}\left(\overline{u_i u_j} - \frac{2}{3}k\delta_{ij}\right) - \alpha\left(P_{ij} - \frac{2}{3}\widetilde{P}\delta_{ij}\right) - \beta\left(D_{ij} - \frac{2}{3}\widetilde{P}\delta_{ij}\right) - \gamma k\left(\frac{\partial U_i}{\partial x_j} + \frac{\partial U_j}{\partial x_i}\right)$$
$$\Pi_{ij,w} = C_1 \frac{\varepsilon}{k}\left(\overline{u_i u_j} - \frac{2}{3}k\delta_{ij}\right) - \frac{\varepsilon}{k}\left(\overline{u_i u_k} n_k n_j + \overline{u_j u_k} n_k n_i\right) - \alpha^*\left(P_{ij} - \frac{2}{3}\widetilde{P}\delta_{ij}\right) \quad (20)$$

where D_{ij} in Eq. (20) is defined by:

$$D_{ij} = \overline{u_i u_k}\frac{\partial U_k}{\partial x_j} + \overline{u_j u_k}\frac{\partial U_k}{\partial x_i}$$

Closures are required for the two viscoelastic contributions on the right hand side of the Reynolds stress transport equation (Eq. (9)), namely for the viscoelastic turbulent transport ($D_{ij,p}$) and the viscoelastic stress work ($\varepsilon_{ij,p}$). The DNS data of Iaccarino et al. (2010) and Masoudian et al. (2013) show that for the whole ranges of tested rheological parameters and Reynolds number, the viscoelastic turbulent transport is negligible in comparison to other terms

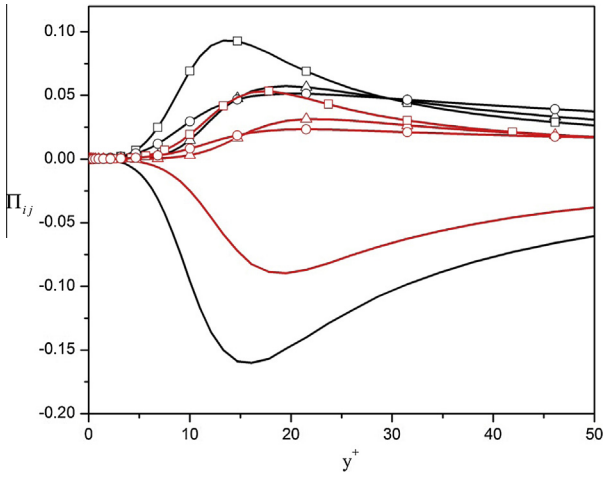

Fig. 8. Prediction of pressure strain term using Eq. (20). Black line: Newtonian, Red line: Viscoelastic case. Solid line: streamwise, □: spanwise, Δ: wall normal, and ○: shear components of pressure strain term. $Re_\tau = 395$, $Wi_\tau = 25$ and $L^2 = 900$. (For interpretation of the references to color in this figure legend, the reader is referred to the web version of this article.)

appearing in the Reynolds stress transport equation and consequently this contribution is neglected in the turbulence model. In contrast, we observed in Section 2 that the viscoelastic stress work is comparable to other contributions, especially far from the wall. It has a similar magnitude to the viscous dissipation and the turbulence production, and it is the main responsible term accounting for the energy transfer with the polymers, consequently developing a closure for this term is required. The viscoelastic stress work appearing in the transport equation of $\overline{u_i u_j}$ is defined as:

$$\varepsilon_{ij,p} = \frac{1}{\rho}\left(\overline{\tau_{ik,p}\frac{\partial u_j}{\partial x_k}} + \overline{\tau_{jk,p}\frac{\partial u_i}{\partial x_k}}\right) = \frac{\eta_p}{\rho\lambda}\left[\underbrace{C_{ik}\overline{f(C_{mm}+c_{mm})\frac{\partial u_j}{\partial x_k}} + C_{jk}\overline{f(C_{mm}+c_{mm})\frac{\partial u_i}{\partial x_k}}}_{term\ 1} + \underbrace{\overline{c_{ik}f(C_{mm}+c_{mm})\frac{\partial u_j}{\partial x_k}} + \overline{c_{jk}f(C_{mm}+c_{mm})\frac{\partial u_i}{\partial x_k}}}_{term\ 2}\right] \quad (21)$$

In order to develop a closure for $\varepsilon_{ij,p}$ we start from its exact definition, Eq. (21). Pinho et al. (2008) and Masoudian et al. (2013) showed that the first two terms on the right hand side of Eq. (21) are negligible in comparison to the remaining triple correlations regardless of the rheological and flow parameters. To model them these triple correlation (last two terms on the right hand side of Eq. (21)) can be decoupled, with good accuracy, into the product of function $f(C_{kk})$ by the remaining double correlation, which is NLT_{ij}. Therefore, the viscoelastic stress work can be calculated by:

$$\varepsilon_{ij,p} \approx \frac{\eta_p}{\rho\lambda} f(C_{mm})\left[\overline{c_{ik}\frac{\partial u_j}{\partial x_k}} + \overline{c_{jk}\frac{\partial u_i}{\partial x_k}}\right] = \frac{\eta_p}{\rho\lambda} f(C_{mm}) NLT_{ij} \quad (22)$$

Fig. 9 compares the predictions of $\varepsilon_{ij,p}$ using Eq. (22) with the corresponding DNS data. Note that neglecting term 1 of Eq. (21) and decoupling the remaining triple correlations (term 2) into the product of function $f(C_{kk})$ by the remaining double correlation are exact assumptions if the Oldroyd-B constitutive equation is considered, which is a limiting case of the FENE-P model for which $f(C_{kk}) = 1$. In other words, the closure developed here for the polymer stress work can also be applied for fluids governed by the Oldroyd-B model. For FENE-P fluids, those assumptions remain valid with a maximum uncertainty of 5%, as depicted in Fig. 9. The joint probability density function of the instantaneous NLT and viscoelastic stress work are calculated using DNS data and plotted for all components at several wall-normal locations in Fig. 10. These quantities are highly correlated for all events, and everywhere across the channel, thus confirming the accuracy of the closure of Eq. (22).

Using the closure developed for $\varepsilon_{ij,p}$ term and substituting it in Eq. (9) the extension of the model of Lai and So (1990) is complete to deal with FENE-P fluids. It is important to emphasize that to capture drag reduction and the influence of polymer additives on the Reynolds-averaged equations only two constant coefficients are added to the original model of Lai and So, namely $a_1 = 0.135$ and $a_2 = 0.1$ for the NLT_{ij} and E_p closures, respectively. A computer optimization algorithm was used to quantify these two constant coefficients.

The remaining constant coefficients and damping functions are those of the original model of Lai and So (1990): $C_1 = 1.5$, $C_2 = 0.4$, $\alpha^* = 0.45$, $C_{\varepsilon 1} = 1.35$, $C_{\varepsilon 2} = 1.8$, $C_s = 0.11$, $\alpha = (8 + C_2)/11$, $\beta = (8C_2 - 2)/11$, $\gamma = (30C_2 - 2)/55$, $f_{w1} = \exp\left[-\left(\frac{R_T}{150}\right)^2\right]$, $f_{w2} = \exp\left[-\left(\frac{R_T}{64}\right)^2\right]$, $f_\varepsilon = 1 - \frac{2}{9}\exp\left[-\left(\frac{R_T}{6}\right)^2\right]$.

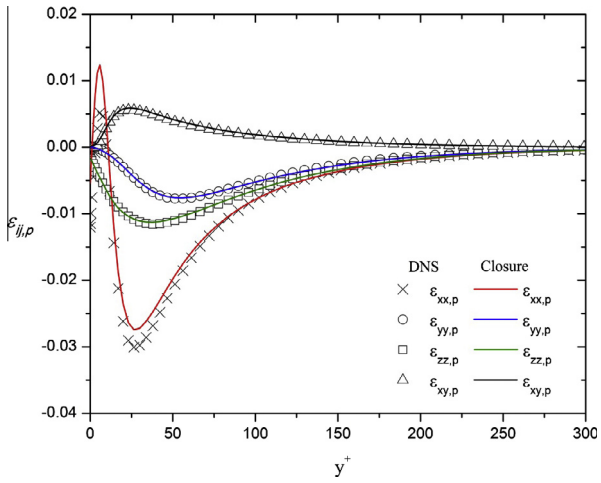

Fig. 9. Comparison between the predictions of $\varepsilon_{ij,p}$ by using the closure developed in Eq. (22), and DNS data for $Re_\tau = 395$, $Wi_\tau = 25$ and $L^2 = 900$.

Note also that a Van-Driest type damping function equal to $(1 - f_{w1})$ was added to the NLT_{ij} closure in order to improve predictions near the wall.

3.3. Summary of the model

Using the closures developed in the previous subsections, the governing and model equations are summarized below.

$$\rho\frac{\partial U_i}{\partial t} + \rho U_k\frac{\partial U_i}{\partial x_k} = -\frac{\partial \overline{P}}{\partial x_i} - \rho\frac{\partial}{\partial x_k}(\overline{u_i u_k}) + \frac{\partial \bar{\tau}_{ik}}{\partial x_k}$$

$$\bar{\tau}_{ij} = 2\eta_s S_{ij} + \bar{\tau}_{ij,p}$$

$$\bar{\tau}_{ij,p} = \frac{\eta_p}{\lambda}[f(C_{kk})C_{ij} - f(L)\delta_{ij}]$$

$$\lambda\left(\left(C_{jk}\frac{\partial U_i}{\partial x_k} + C_{ik}\frac{\partial U_j}{\partial x_k}\right) + NLT_{ij}\right) = [f(C_{kk})C_{ij} - f(L)\delta_{ij}]$$

$$\frac{\partial \overline{u_i u_j}}{\partial t} + U_k\frac{\partial \overline{u_i u}}{\partial x_k} = \left(-\overline{u_i u_k}\frac{\partial U_j}{\partial x_k} - \overline{u_j u_k}\frac{\partial U_i}{\partial x_k}\right) + D_{ij,\upsilon} + D_{ij,t} + \varepsilon_{ij} + \Pi_{ij} - \varepsilon_{ij,p}$$

$$\frac{D\varepsilon}{Dt} = \frac{\partial}{\partial x_k}\left(\upsilon\frac{\partial \varepsilon}{\partial x_k}\right) + \frac{\partial}{\partial x_k}\left(C_s\frac{k}{\varepsilon}\overline{u_k u_i}\frac{\partial \varepsilon}{\partial x_i}\right) + C_{\varepsilon 1}(1 + \sigma f_{w,2})\frac{\varepsilon}{k}\widetilde{P} - C_{\varepsilon 2}f_\varepsilon \times \frac{\varepsilon\tilde{\varepsilon}}{k} + f_{w,2}\left[\left(\frac{7}{9}C_{\varepsilon 2} - 2\right)\frac{\varepsilon\tilde{\varepsilon}}{k} - \frac{1}{2k}\left(\varepsilon - \frac{2\upsilon k}{y^2}\right)^2\right] - E_p$$

where the specific terms and closures associated with the FENE-P fluid are:

$$NLT_{ij} = a_1(1 - f_{w1})\frac{\lambda}{\upsilon_p}\frac{\varepsilon}{k}\frac{Wi_h\sqrt{L}}{f(C_{kk})}\overline{u_i u_j}, \quad a_1 = 0.135$$

$$\varepsilon_{ij,p} = \frac{\eta_p}{\rho\lambda}f(C_{mm})NLT_{ij}$$

$$E_p = a_2\varepsilon_{ii,p}\frac{\varepsilon}{k}, \quad a_2 = 0.1$$

4. Results and discussion

In this section, predictions using the developed closures are presented for fully-developed turbulent channel flow of FENE-P fluids. The closures are assessed against the DNS data for FENE-P fluids. All viscoelastic flow calculations were carried out using the same flow conditions as for the DNS.

The computer code used for the present model calculation is based on a finite-volume method using a second-order central difference schemes on a staggered mesh. The Tri-Diagonal Matrix Algorithm (TDMA) solver is used to calculate the solution of the discretised algebraic governing equations. The non-uniform mesh consists of 99 cells across the channel, giving mesh independent results for the low drag reduction case with 0.1% uncertainty in drag reduction prediction (Table 2). The full domain is mapped exclusively in the transverse direction, hence only the following wall boundary condition needs to be imposed on both walls:

$$U_i = 0, \ \overline{u_i u_j} = 0, \quad \text{and} \quad \varepsilon = 2\upsilon\left(\frac{\partial\sqrt{k}}{\partial y}\right)^2$$

4.1. Channel flow prediction for low and high drag reduction cases

Predicted transverse profiles of the mean streamwise velocity are plotted in Fig. 11, along with the corresponding DNS predictions. In the viscous sublayer the velocity profiles collapse on the linear distribution $U^+ = y^+$ as they should. Further away from the wall, as expected, the mean velocity of the drag reduced flows increases, and the logarithmic profile shifts upwards but remains parallel to that of the Newtonian flow as is also found in the DNS results. The upward shift of the logarithmic profile can be interpreted as a thickening of the buffer layer in agreement with the experimental and numerical findings of Ptasinski et al. (2003) and Li et al. (2006).

The corresponding predictions of the dimensionless u_{rms}, v_{rms}, w_{rms}, and $\overline{uv}$ profiles are shown in Fig. 12, and compared with the corresponding DNS profiles for low DR (LDR) and high DR (HDR) in Fig. 12(a) and (b), respectively. It is well known (Ptasinski et al., 2003; Li et al., 2006) that streamwise velocity fluctuations u_{rms} increase slightly with DR, while the wall-normal and spanwise components monotonically decrease. Moreover the peak location of u_{rms} shifts away from the wall as DR increases, which is consistent with the upward shift of the logarithmic region in the mean velocity profile. Fig. 12(a) compares the DNS and predictions of u_{rms}, v_{rms}, w_{rms} and $\overline{uv}$ profiles for LDR and as it can be seen, except for u_{rms} the predictions are in good agreement with DNS results, with the model being capable of capturing the suppression of wall-normal and spanwise turbulent intensities which is inherent to turbulent DR with dilute polymer solutions. Moreover $\overline{uv}$ is in good agreement with DNS results, and the proposed model predicts very well both the reduction in magnitude of the stress and the shift of the location of its peak value. The predictions of u_{rms}, v_{rms}, w_{rms}, and $\overline{uv}$ along with DNS results for HDR regimes, DNS9, are plotted in Fig. 12(b). It is well known that for the HDR cases v_{rms}, w_{rms} and $\overline{uv}$ decrease until around 30% of the corresponding Newtonian values. As it can be seen in Fig. 12(b) the predictions of these suppressions of v_{rms}, w_{rms} and $\overline{uv}$ are well captured by the present model, also confirming that the Newtonian closure developed by Lai and So for the pressure strain term is also capable of predicting well in viscoelastic fluids. However, in both cases the model under-predicts u_{rms}, but it should be noted that this under prediction of u_{rms} is arguably somewhat fictitious: in the experiments of Ptasinski et al. (2003) the streamwise turbulence (u_{rms}) increases slightly by increasing DR. On the other hand their corresponding DNS results over-predict those peak values i.e., DNS with the FENE-P constitutive equation predicts higher values of u_{rms} than is usually measured with real fluids. They extensively discuss this difference and state that this might be due to shortcomings in the FENE-P

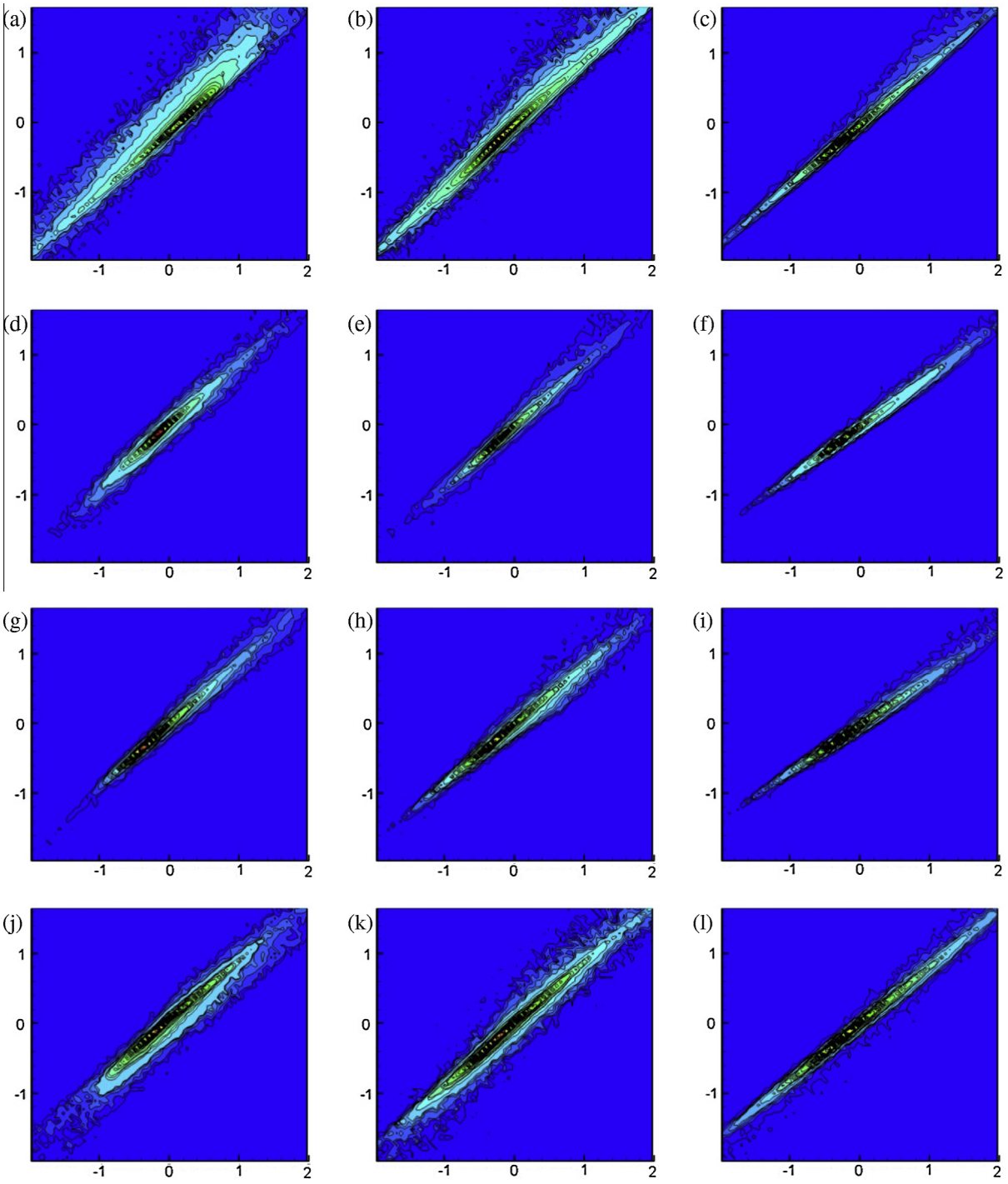

Fig. 10. Joint PDF of (a) NLT_{xx}, $\varepsilon_{xx,p}$ at $y^+ = 5$, (b) NLT_{xx}, $\varepsilon_{xx,p}$ at $y^+ = 15$, (c) NLT_{xx}, $\varepsilon_{xx,p}$ at $y^+ = 75$, (d) NLT_{yy}, $\varepsilon_{yy,p}$ at $y^+ = 5$, (e) NLT_{yy}, $\varepsilon_{yy,p}$ at $y^+ = 15$, (f) NLT_{yy}, $\varepsilon_{yy,p}$ at $y^+ = 75$, (g) NLT_{zz}, $\varepsilon_{zz,p}$ at $y^+ = 5$, (h) NLT_{zz}, $\varepsilon_{zz,p}$ at $y^+ = 15$, (i) NLT_{zz}, $\varepsilon_{zz,p}$ at $y^+ = 75$, (j) NLT_{xy}, $\varepsilon_{xy,p}$ at $y^+ = 5$, (k) NLT_{xy}, $\varepsilon_{xy,p}$ at $y^+ = 15$, (l) NLT_{xy}, $\varepsilon_{xy,p}$ at $y^+ = 75$, for DNS data described as: $Re_{\tau 0} = 395$, $Wi_{\tau 0} = 25$ and $L^2 = 900$.

Table 2
Mesh independency analyses.

Grid points across the channel	Predicted drag reduction	DNS (%)
59	Diverged	18
79	14.1	18
99	16.2	18
199	16.2	18

model. An extensive discussion can be found in Ptasinski et al. (2003).

The overall shear stress balances for the low and high DR cases are plotted in Fig. 13 using wall coordinates. It includes the Reynolds stress, the solvent stress, and the polymer stress. In a fully developed flow condition, the total shear stress, the sum of the Reynolds, solvent, and polymer stresses, must follow a straight line across the channel varying from zero at the centerline to the wall shear stress at the wall. Here, the total shear stress is the sum of three contributions, namely, the Reynolds stress, the

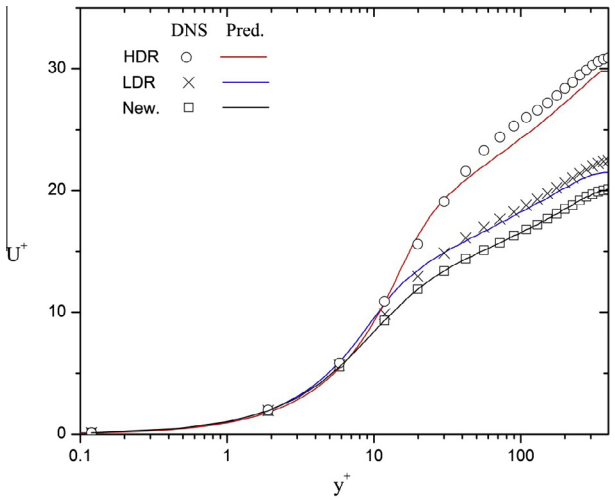

Fig. 11. Transverse profiles of the mean streamwise velocity in wall coordinates, LDR: case DNS5, HDR: case DNS9.

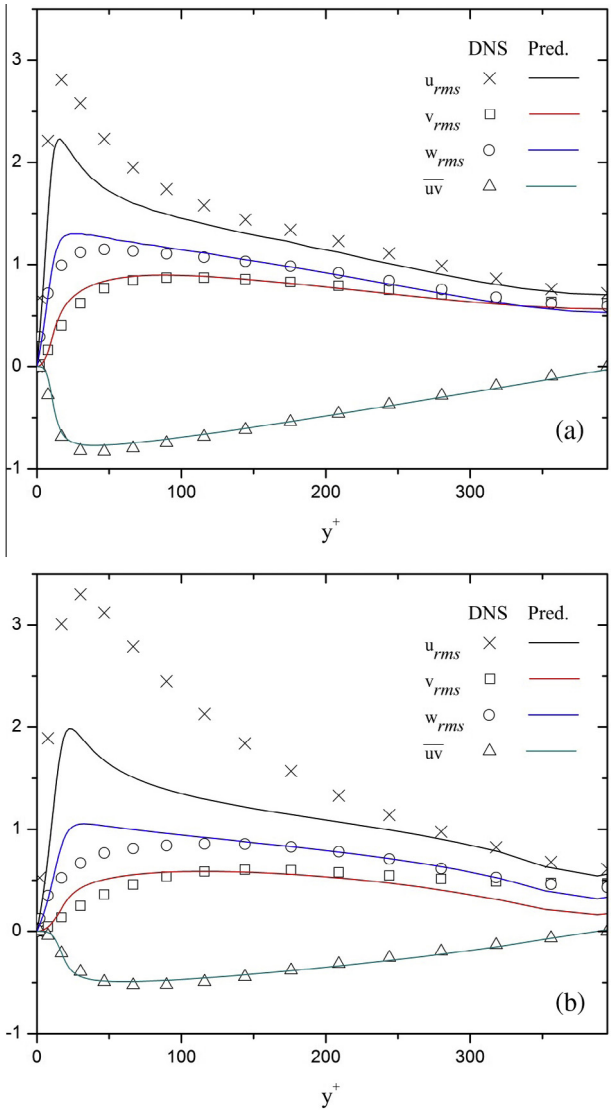

Fig. 12. Transvers profiles of the of u_{rms}, v_{rms}, w_{rms} and $\overline{uv}$, (a) LDR (case DNS5), and (b) HDR (case DNS9).

solvent viscous stress and the polymer stress. All stresses are normalized by the wall shear stress for low and high DR and compared with the corresponding DNS. For both LDR and HDR the total shear stress follows the expected linear profiles over the channel height, indicating that a stationary fully developed state has been reached. In the low drag reduction case the polymer stress contribution is relatively small, and it occurs mainly in the near wall region. However, as DR increases, the Reynolds stress is significantly reduced, and correspondingly the polymer stress increases to ensure the balance, thus becoming comparable to the Reynolds stress, specifically at HDR. In both cases the proposed model predicts the peak and the general trend of the Reynolds stresses, the solvent stresses, and the polymer stresses very well. These observations are also consistent with the numerical findings of Li et al. (2006) and the experimental results of Ptasinski et al. (2003).

Predictions of the Peterlin function and of the trace of the polymer length, normalized by its possible maximum extension length (L^2) are compared with DNS data for the low and high DR cases in Fig. 14. In both cases the predictions are in good agreement with the DNS data. In agreement with findings of Li et al. (2006), the region of high chain dumbbell extension is limited to the near wall region ($y^+ < 50$) and the developed model is predicting well these quantities near and far from the wall.

The performance of this new model is evaluated next against existing turbulence for FENE-P fluids. As reviewed in the

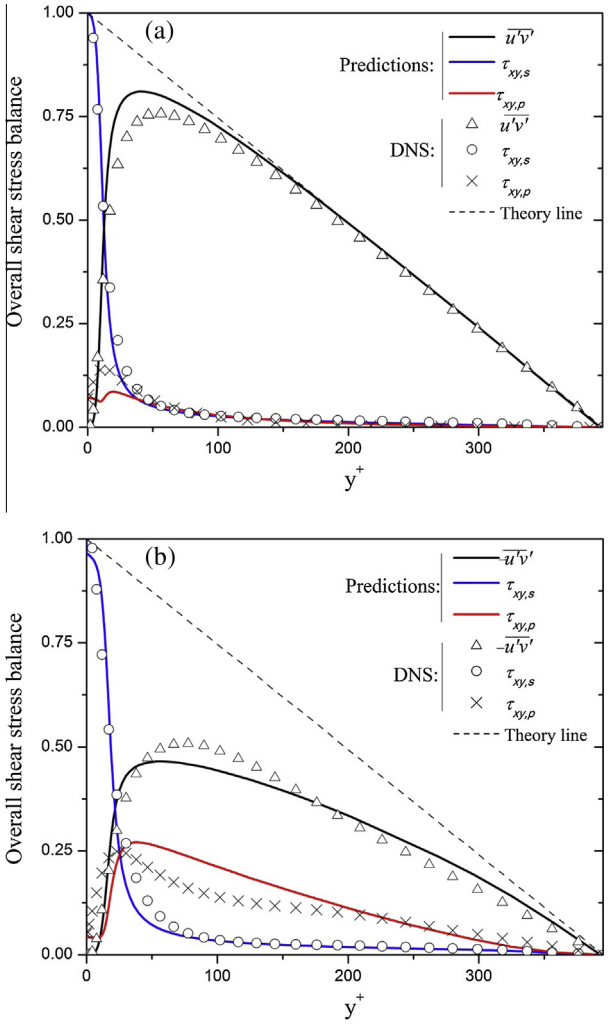

Fig. 13. Predictions of overall stress balance, (a) LDR (case DNS5), and (b) HDR (case DNS9).

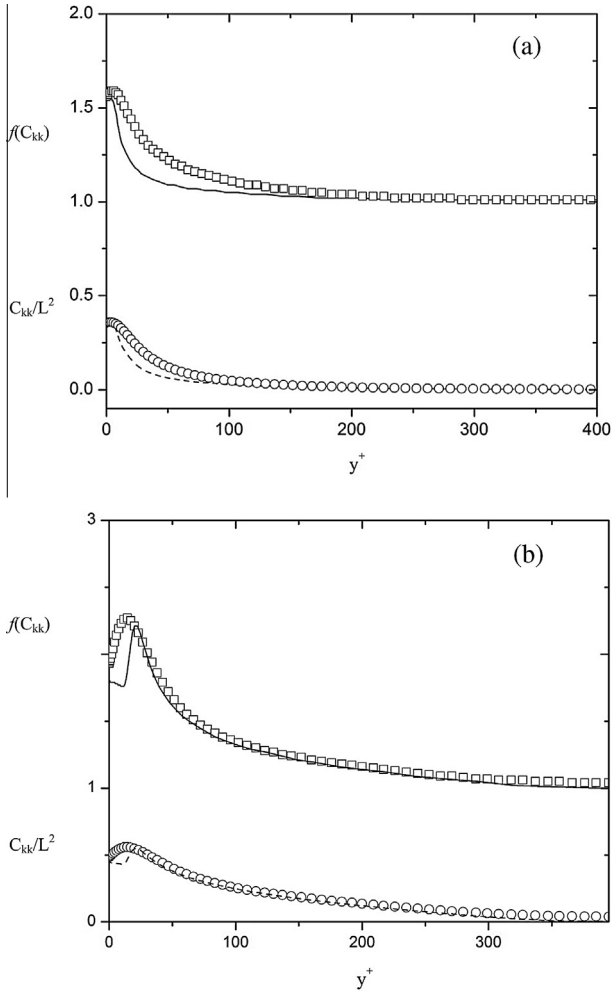

Fig. 14. Transverse profiles of the $f(C_{kk})$, and C_{kk}/L^2. □: DNS of $f(C_{kk})$, ○: DNS of C_{kk}/L^2 dash line: predictions of C_{kk}/L^2, solid line: predictions of $f(C_{kk})$. (a) LDR (case DNS5), and (b) HDR (case DNS9).

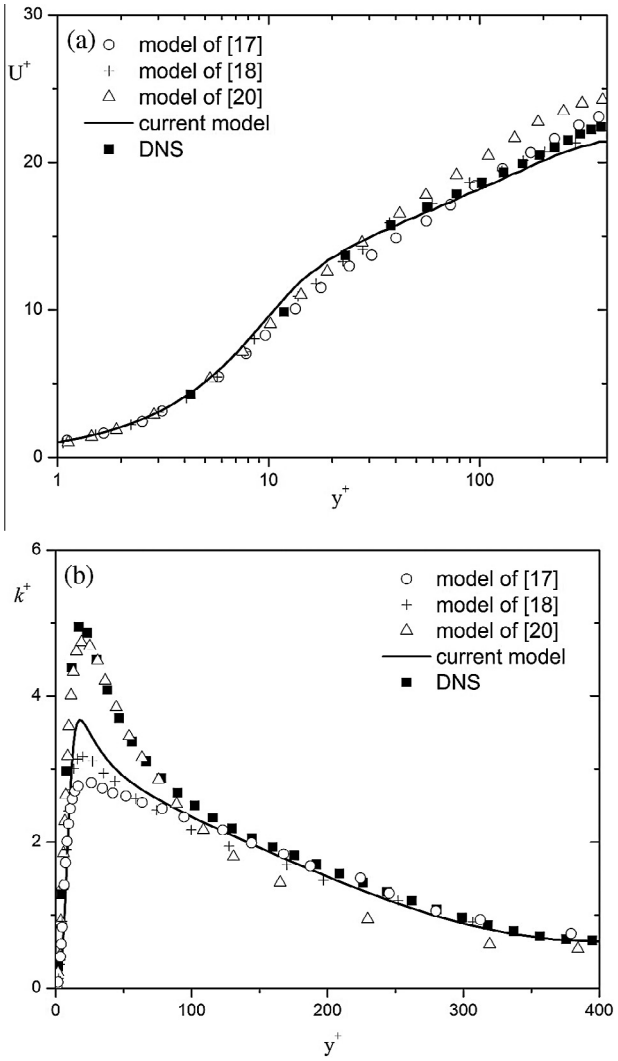

Fig. 15. Comparison of current RS model with previous models developed for FENE-P fluids, (a) mean velocity profile, and (b) turbulent kinetic energy (case DNS5).

Introduction, the first k–ε based turbulence model for FENE-P fluids was developed by Pinho et al. (2008). This early model is only capable of predicting LDR flows, and contains three new damping functions and five constant coefficients. Subsequent development by Resende et al. (2011) resulted in a very complex model, with circa twenty new tunable parameters among coefficients and damping functions, and was only valid for low and intermediate DRs. The best of those earliest models for FENE-P fluids were developed in the context of the k–ε–$\overline{v^2}$–f first by Iaccarino et al. (2010) and then by Masoudian et al. (2013). Both models are valid up to the maximum DR, containing only three new constant coefficients.

In Fig. 15, the normalized mean velocity and turbulent kinetic energy predicted by the current model are compared with the corresponding predictions by the earlier models of Pinho et al. (2008), Resende et al. (2011) and Masoudian et al., 2013. Note that the present model only has two additional constant coefficients compared with the base Newtonian RSM model, whereas the earlier models have more new terms coefficients than their base Newtonian models. The second-order Reynolds stress model developed here predicts better the mean velocity profile all across the channel, whereas for the turbulent kinetic energy it predicts better than the models of Pinho et al. (2008) and Resende et al., 2011, but it is outperformed by the model of Masoudian et al. (2013). However, note the worse prediction of Masoudian et al. (2013) in terms of the mean velocity profile so that overall the current model is judged as a better turbulence model. Nevertheless, as discussed above, the higher peak of k calculated by DNS comes from the over prediction of the streamwise Reynolds stress, which is likely to be due to drawbacks of the FENE-P model. In addition, the current second order RS model is theoretically capable of better performance in other more complex flows especially involving secondary

Table 3
Overall drag reduction prediction and comparison with independent DNS results.

Reference DNS	$Re_{\tau 0}$	Rheological parameters		Drag reduction	
		$Wi_{\tau 0}$	L^2	DNS (%)	Current model (%)
Li et al. (2006)	125	25	900	18	19
Iaccarino et al. (2010)	300	36	10,000	35	34
Iaccarino et al. (2010)	300	60	3600	47	44
Iaccarino et al. (2010)	300	36	19,600	32	32
Iaccarino et al. (2010)	300	36	3600	33	33
Iaccarino et al. (2010)	300	60	19,600	42	41
Li et al. (2006)	395	25	3600	19	20
Li et al. (2006)	395	50	3600	38	36
Li et al. (2006)	395	75	3600	44	44
Li et al. (2006)	395	100	14,400	61	60
Li et al. (2006)	395	75	900	34	31
Thais et al. (2013)	1000	50	900	30	31

Table 4
Different values of damping function (f_{w1}) in closure of NLT.

Run	Dapping function
Optimized model	$f_{w1} = \exp\left[-\left(\frac{R_t}{150}\right)^2\right]$
(a)	Without damping
(b)	$f_{w1} = \exp\left[-\left(\frac{R_t}{100}\right)^2\right]$
(c)	$f_{w1} = \exp\left[-\left(\frac{R_t}{200}\right)^2\right]$

Table 5
Different values of constant coefficient (a_1) in closure of *NLT*.

Run	a_1
Optimized model	0.135
(d)	0.15
(e)	0.17
(f)	0.1
(g)	0.115

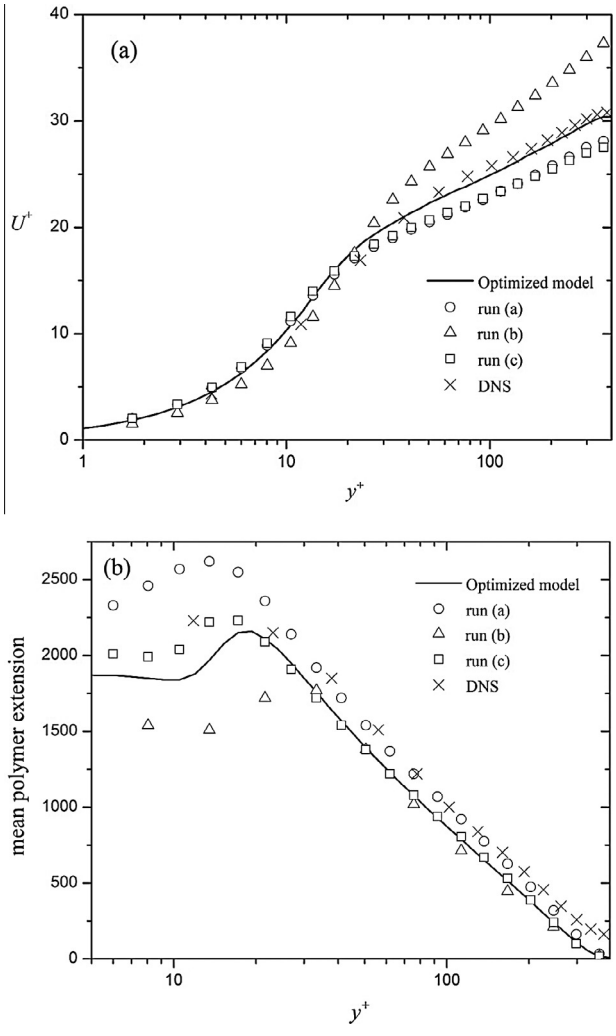

Fig. 16. Influence of the utilized damping function in *NLT* closure on (a) mean velocity profile (b) mean polymer length (C_{kk}) for HDR case (case DNS9). See Table 4 for detail about runs (a), (b), (c), and optimized model.

flows, flow separation or 3D flow, where all components of the Reynolds stress tensor play a role. This is the topic of future research as it needs also the availability of the corresponding DNS data for assessment.

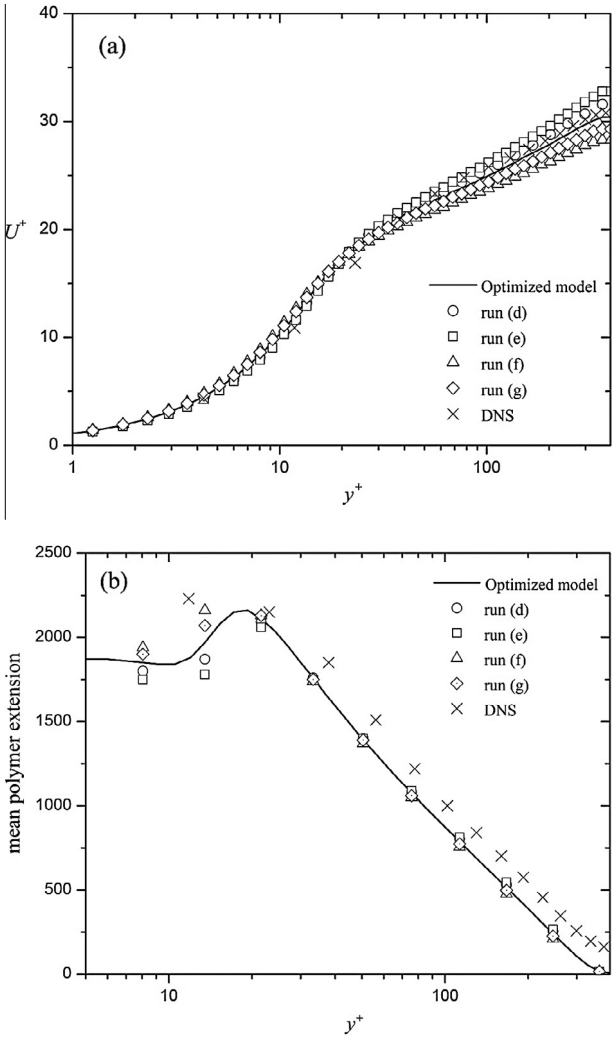

Fig. 17. Influence of the utilized constant coefficient, a_1, in *NLT* closure on (a) mean velocity profile (b) mean polymer length (C_{kk}) for HDR case (case DNS9). See Table 5 for detail about runs (d), (e), (f), (g), and optimized model.

The present model compares well with the DNS data in terms of overall drag reduction; for total twelve cases of independent DNS results (Li et al., 2006; Iaccarino et al., 2010; Thais et al., 2013) listed in Table 3, the predicted DR values by the present model are fairly in good agreement with DNS results for a wide range of Reynolds number ($125 < Re < 1000$) with different amounts of drag reduction, which shows the robustness of the model.

In order to investigate the sensitivity of the *NLT* closure to the choice of the model constant (a_1) and wall damping function ($1 - f_{w1}$), several values and expressions for these quantities were tested independently, as listed in Tables 4 and 5 for f_{w1} and a_1, respectively. The corresponding predictions assessed through transverse profiles of the mean polymer extension (C_{kk}) and mean velocity profiles, the objective functions in the optimization process. These results are shown in Figs. 16 and 17 for f_{w1} and a_1, respectively. It is clear that the best predictions are obtained with the optimum expression and value of the damping function and coefficient introduced above.

Although the present closures for the non-linear term in the constitutive equation and for the polymer stress work in the transport equation for the Reynolds stress were developed in the context of the RSM model of Lai and So (1990), they were inspired and are extensions of earlier closures developed in the context of earlier models. These and their good near wall predicting

capabilities of turbulent statistics suggest that their use with a different Reynolds stress base model, such as the model of Speziale et al. (1991), only requires minor changes in the closures to account for the correct influence of polymer additives on the flow.

5. Conclusion

A low-Reynolds-number second-order Reynolds stress model was developed to predict turbulent flow of homogeneous polymer solutions described by the FENE-P constitutive equation. The model is an adaptation of the Reynolds stress model of Lai and So (1990) for Newtonian fluids, it is here used for predictions of turbulent channel flow and represents a significant improvement over the previous second-order RS model of Leighton et al. (2003), which was limited to low drag reduction in spite of a large number of coefficient. The assessment of its performance in other canonical turbulent flows is the subject of future research as it requires DNS and/or experimental data in such flows as wall free jets or recirculating flows.

Thirteen sets of DNS data were analyzed to investigate budgets of the Reynolds stress transport equation and of the time-averaged FENE-P constitutive equation. The developed closure for the turbulent nonlinear distortion term of the conformation tensor (*NLT*) is based on the rheological and turbulent flow parameters. In addition, closures are also developed for the viscoelastic stress work, which shows its robustness through a series of comparisons of its instantaneous and mean values. It was not necessary to develop a specific closure for the pressure strain, so its computation relies on the closure of Lai and So (1990).

The performance of the present model is assessed against a large number of DNS data, including independent sets from the literature and covers a wide range of flow and rheological conditions ($125 < Re_{\tau 0} < 1000$, $25 < Wi_{\tau 0} < 100$, $900 < L^2 < 19{,}600$). This assessment also includes predictions by earlier turbulence models for fully developed viscoelastic channel flow.

The predictions in fully-developed channel flow compare very well with DNS data in terms of mean velocity, turbulent kinetic energy and viscoelastic stresses at all ranges of drag reduction. The turbulence model developed here uses the same wall damping functions as the original model of Lai and So (1990) and the new closures required to account for viscoelastic fluid behavior are simple, numerically inexpensive and stable with the model showing effectively a good predictive capability for FENE-P fluids.

Acknowledgements

Financial support provided by Fundação para a Ciência e a Tecnologia (FCT), COMPETE and FEDER through project PTDC/EME-MFE/113589 is gratefully acknowledged by M. Masoudian and F.T. Pinho. R. Sureshkumar gratefully acknowledges support from the US National Science Foundation through grant CBET1055219. K. Kim gratefully acknowledges support from National Research Foundation of South Korea (NRF-2014K2A1A2048497).

References

Dimitropoulos, C.D., Dubief, Y., Shaqfeh, E.S., Moin, P., Lele, S.K., 2005. Direct numerical simulation of polymer-induced drag reduction in turbulent boundary layer flow. Phys. Fluids (1994-present) 17 (1), 011705.

Dubief, Y., White, C.M., Terrapon, V.E., Shaqfeh, E.S., Moin, P., Lele, S.K., 2004. On the coherent drag-reducing and turbulence-enhancing behaviour of polymers in wall flows. J. Fluid Mech. 514, 271–280.

Hoyt, J.W., 1972. A freeman scholar lecture: the effect of additives on fluid friction. J. Fluids Eng. 94 (2), 258–285.

Iaccarino, G., Shaqfeh, E.S., Dubief, Y., 2010. Reynolds-averaged modeling of polymer drag reduction in turbulent flows. J. Nonnewton. Fluid Mech. 165 (7), 376–384.

Lai, Y.G., So, R.M.C., 1990. On near-wall turbulent flow modeling. J. Fluid Mech. 221, 641–673.

Leighton, R., Walker, D.T., Stephens, T., Garwood, G., 2003. Reynolds stress modeling for drag reducing viscoelastic flows. In: ASME/JSME 2003 4th Joint Fluids Summer Engineering Conference. American Society of Mechanical Engineers, pp. 735–744.

Li, C.F., Sureshkumar, R., Khomami, B., 2006. Influence of rheological parameters on polymer induced turbulent drag reduction. J. Nonnewton. Fluid Mech. 140 (1), 23–40.

Lumley, John L., 1969. Drag reduction by additives. Annu. Rev. Fluid Mech. 1 (1), 367–384.

Lumley, J.L., 1973. Drag reduction in turbulent flow by polymer additives. J. Polym. Sci. 7, 263–290.

Malin, M.R., 1998. Turbulent pipe flow of Herschel–Bulkley fluids. Int. Commun. Heat Mass Transfer 25 (3), 321–330.

Masoudian, M., Kim, K., Pinho, F.T., Sureshkumar, R., 2013. A viscoelastic turbulent flow model valid up to the maximum drag reduction limit. J. Nonnewton. Fluid Mech. 202, 99–111.

Oliver, T.A., Malaya, N., Ulerich, R., Moser, R.D., 2014. Estimating uncertainties in statistics computed from direct numerical simulation. Phys. Fluids (1994-present) (263), 035101.

Pinho, F.T., 2003. A GNF framework for turbulent flow models of drag reducing fluids and proposal for a k–ε type closure. J. Nonnewton. Fluid Mech. 114 (2), 149–184.

Pinho, F.T., Li, C.F., Younis, B.A., Sureshkumar, R., 2008. A low Reynolds number turbulence closure for viscoelastic fluids. J. Nonnewton. Fluid Mech. 154 (2), 89–108.

Poole, R.J., Escudier, M.P., 2003. Turbulent flow of non-Newtonian liquids over a backward-facing step: Part II. Viscoelastic and shear-thinning liquids. J. Nonnewton. Fluid Mech. 109 (2), 193–230.

Poreh, M., 1978. Turbulent energy dissipation model for fins with drag reduction. J. Fluids Eng. 100, 107.

Ptasinski, P.K., Boersma, B.J., Nieuwstadt, F.T.M., Hulsen, M.A., Van den Brule, B.H.A.A., Hunt, J.C.R., 2003. Turbulent channel flow near maximum drag reduction: simulations, experiments and mechanisms. J. Fluid Mech. 490, 251–291.

Resende, P.R., Kim, K., Younis, B.A., Sureshkumar, R., Pinho, F.T., 2011. A FENE-P k–ε turbulence model for low and intermediate regimes of polymer-induced drag reduction. J. Nonnewton. Fluid Mech. 166 (12), 639–660.

Resende, P.R., Pinho, F.T., Cruz, D.O., 2013. A Reynolds stress model for turbulent flows of viscoelastic fluids. J. Turbul. 14 (12), 1–36.

Shima, N., 1988. A Reynolds-stress model for near-wall and low-Reynolds-number regions. J. Fluids Eng. 110 (1), 38–44.

Speziale, C.G., Sarkar, S., Gatski, T.B., 1991. Modelling the pressure–strain correlation of turbulence: an invariant dynamical systems approach. J. Fluid Mech. 227, 245–272.

Sureshkumar, R., Beris, A.N., Handler, Robert A., 1997. Direct numerical simulation of the turbulent channel flow of a polymer solution. Phys. Fluids (1994-present) 9 (3), 743–755.

Tabor, M., De Gennes, P.G., 1986. A cascade theory of drag reduction. EPL (Europhys. Lett.) 2 (7), 519.

Thais, L., Tejada-Martinez, A.E., Gatski, T.B., Mompean, G., 2010. Temporal large eddy simulations of turbulent viscoelastic drag reduction flows. Phys. Fluids (1994-present) 22 (1), 013103.

Thais, L., Gatski, T.B., Mompean, G., 2013. Analysis of polymer drag reduction mechanisms from energy budgets. Int. J. Heat Fluid Flow 43, 52–61.

Toms, Be A., (1948). Some observations on the flow of linear polymer solutions through straight tubes at large Reynolds numbers. In: Proceedings of the 1st International Congress on Rheology, vol. 2.

Tsukahara, T., Kawaguchi, Y., 2013. Proposal of damping function for low-Reynolds-number-model applicable in prediction of turbulent viscoelastic-fluid flow. J. Appl. Math.

Virk, P.S., 1971. An elastic sublayer model for drag reduction by dilute solutions of linear macromolecules. J. Fluid Mech. 45 (03), 417–440.

Virk, P.S., 1975. Drag reduction fundamentals. AIChE J. 21 (4), 625–656.